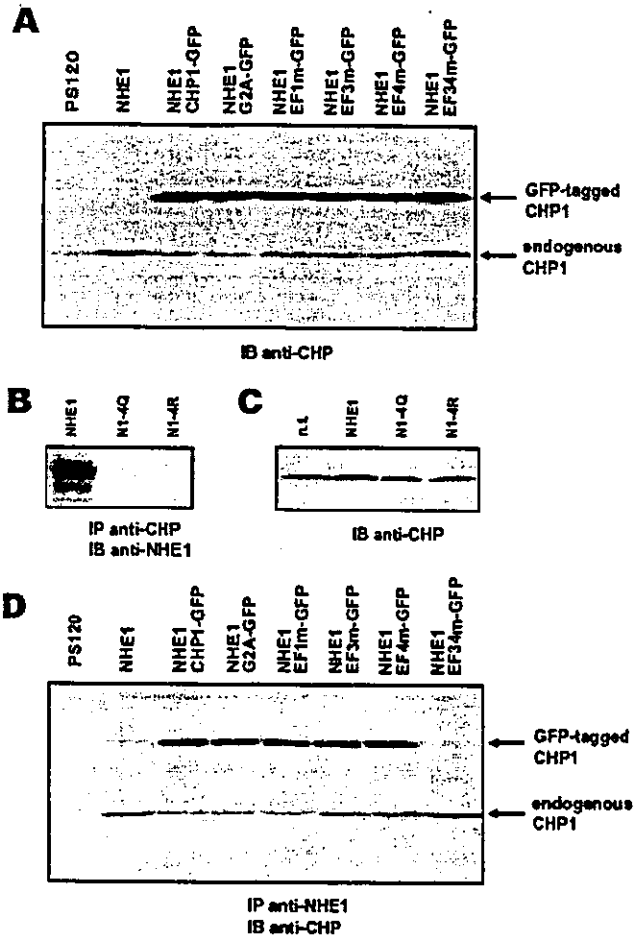

FIGURE 4: Expression of various GFP-tagged CHP1 proteins and their coimmunoprecipitation with NHE1. Panel A shows the expression level of GFP-tagged CHP1 and its variants (indicated at the top of the figure). Cell lysates (50 μg) from stable transfectants were subjected to SDS–PAGE, and expression of endogenous and exogenous CHP1 proteins were detected by immunoblotting (IB) with an anti-CHP1 antibody. A result for untransfected PS120 cells is shown in the first lane. Panel B shows coimmunoprecipitation of the wild-type or mutant (4Q and 4R) exchangers with endogenous CHP1. Lysates from cells stably expressing these exchangers were subjected to immunoprecipitation with anti-CHP1 antibody followed by immunoblotting with anti-NHE1 antibody. Panel C shows the expression level of endogenous CHP1 in cells expressing the wild-type or mutant NHE1s: n.t., no transfection. Panel D shows coimmunoprecipitation of CHP1 proteins with NHE1. Lysates from cells stably expressing various proteins were subjected to immunoprecipitation with anti-NHE1 antibody followed by immunoblotting with anti-CHP1 antibody. Note that in lanes from cells not transfected with GFP-tagged CHP1 (left two lanes), IgG protein bands were visible at the same positions as GFP-tagged CHP1.

CHP1 complexed with the NHE1 fragment ($t_{1/2} = \sim 7$ s) was much slower. A slow release of $^{45}Ca^{2+}$ also occurred in two mutant CHP1 proteins, EF3m and EF4m, complexed with the NHE1 fragment (Figure 3B), suggesting that Ca^{2+} binds tightly to each EF hand.

Effects of CHP1 Mutations on NHE1 Regulation. To study the role of Ca^{2+} binding in NHE1 regulation by CHP1, we transfected GFP-tagged CHP1 into cells expressing NHE1 and obtained cells stably coexpressing these proteins. The results indicated that GFP-tagged CHP1 and its mutant derivatives were highly coexpressed in NHE1 transfectants (Figure 4A). Interestingly, expression of NHE1 markedly increased the level of expression of the endogenous CHP1 (3.6-fold), while coexpression of various GFP-tagged CHP1 variants, with the exception of CHP1-EF34m-GFP, reduced it (Table 2).

Table 2: Relative Amounts of Expressed GFP-Tagged CHP1 and Endogenous CHP1

transfected proteins	relative amount of GFP-tagged CHP1[a]	relative amount of endogenous CHP[b]
untransfected		1.00 ± 0.08
NHE1		3.63 ± 0.81[c]
NHE1 + CHP1-GFP	1.00 ± 0.11	1.11 ± 0.13
NHE1 + G2A-GFP	1.08 ± 0.11	1.03 ± 0.16
NHE1 + EF1m-GFP	0.93 ± 0.06	1.07 ± 0.11
NHE1 + EF3m-GFP	0.97 ± 0.11	1.15 ± 0.16
NHE1 + EF4m-GFP	1.06 ± 0.07	1.09 ± 0.10
NHE1 + EF34m-GFP	0.94 ± 0.12	3.85 ± 0.45[c]
NHE1-4Q		1.02 ± 0.09
NHE1-4R		1.03 ± 0.06

[a] The density of visualized protein bands on immunoblots (cf. Figure 4, panels A and C) is represented as values normalized according to the band density from cells expressing CHP1-GFP. Data are means ± SD ($n = 3$). [b] The band density is represented as values normalized according that from untransfected PS120 cells. Data are means ± SD ($n = 3$). [c] $P < 0.05$ versus control.

We further examined the effect of expression of CHP1 binding-defective NHE1 mutants 4Q and 4R on the amount of endogenous CHP. These mutant exchangers do not bind CHP1 as shown by coimmunoprecipitation studies (Figure 4B). The level of expression of the endogenous CHP1 did not increase on coexpression of these mutant exchangers (Figure 4B,C, Table 2). Thus, the amount of endogenous CHP1 in cells is highly dependent on expression of NHE1 and GFP-tagged CHP1.

Figure 4D shows the results for coimmunoprecipitation experiments using NHE1- and CHP1-specific antibodies to determine interactions of the expressed CHP1–GFP with NHE1. Anti-NHE1 antibody immunoprecipitated endogenous CHP1 from cells expressing NHE1. In cells coexpressing GFP–CHP1 and NHE1, the same antibody coimmunoprecipitated large quantities of GFP–CHP1 or its derivatives, and at the same time, the amount of immunoprecipitated endogenous CHP1 was markedly reduced. In cells coexpressing EF34m–GFP and NHE1, anti-NHE1 antibody coimmunoprecipitated the endogenous CHP1 but not exogenous GFP-tagged mutant CHP1, consistent with the findings of in vitro binding studies indicating that double mutation at EF3 and EF4 impairs the interaction of CHP1 with NHE1.

We next examined the subcellular localization of GFP-tagged CHP1. As reported previously (*12*), the GFP-tagged CHP1 is localized in the plasma membrane in cells coexpressing NHE1 (Figure 5A). Consistent with the in vitro binding data (Figure 1B), the GFP fluorescence was observed in the plasma membrane in cells coexpressing GFP-tagged CHP1 mutants except EF34m with NHE1 (Figure 5A; data not shown for G2A and EF1m). These results, together with the data from coimmunoprecipitation experiments, indicate that the endogenous CHP1 bound to NHE1 was efficiently replaced by expressed GFP-tagged wild-type or CHP1 mutants. However, the double mutant EF34m was not localized at the plasma membrane (Figure 5A) because of the weak interaction of this mutant protein with the juxtamembrane region of NHE1. We observed that GFP fluorescence was still observed in the plasma membrane after addition of phorbol ester, serum, thrombin, lysophosphatidic

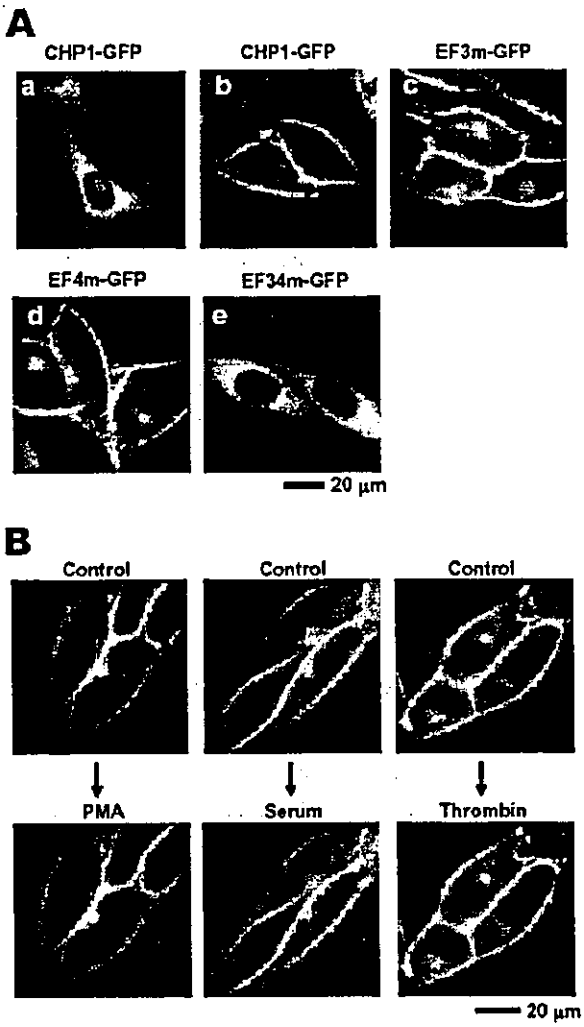

FIGURE 5: Subcellular localization of GFP-tagged CHP1: (A) subcellular localization of GFP-tagged wild-type CHP1 (a, b), EF3m (c), EF4m (d), and EF34m (e) expressed in PS120 cells (a) or in their stable transfectants of the wild-type NHE1 (b–e); (B) effect of various agents on the subcellular localization of the wild-type GFP-tagged CHP1 in NHE1 transfectants. Cells were placed in serum-free Dulbecco's modified Eagle's medium without phenol red for 5 h, and then 1 μM PMA, 10% serum, or 2 units/ml thrombin were added. GFP fluorescence was observed under a fluorescent microscope equipped with a CoolSNAP imaging system (RS Photometrics) before (control) and 20 min after addition of the various agents.

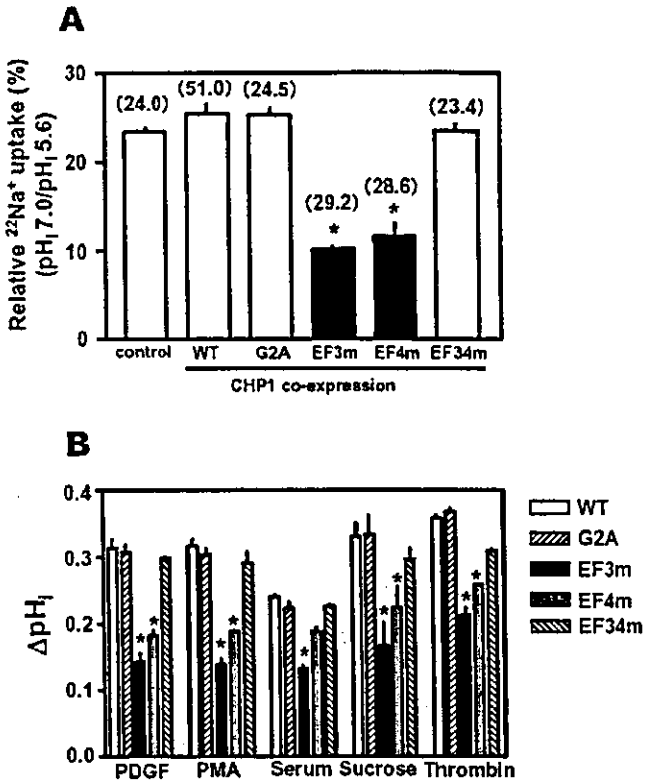

FIGURE 6: Exchange activity and regulation of NHE1 transfectants expressing various CHP1 mutants. Panel A shows ratios of EIPA-sensitive $^{22}Na^+$ uptake activities of cells coexpressing wild-type NHE1 and various CHP1 mutants at pH$_i$ 7.0 and 5.6. Numbers (nmol/mg/min) in parentheses represent $^{22}Na^+$ uptake activity at pH$_i$ = 5.6. Control cells were not transfected with CHP1 but stably expressing NHE1. Data are means ± SD (n = 3; *, P < 0.05 versus cells not expressing exogenous CHP1). Panel B shows changes in pH$_i$ measured using the [^{14}C]benzoic acid equilibration method. The cells coexpressing NHE1 and various CHP1 variants were stimulated for 15 min at 37 °C with 10 ng/mL PDGF-BB, 1 μM PMA, 10 μg/mL lysophosphatidic acid, or 200 mM sucrose (hyperosmotic stress). Data are means ± SD (n = 6; *, P < 0.05 versus cells expressing wild-type CHP1).

acid, or PDGF-BB, which are all known to activate the exchange activity (Figure 5B, data not shown for some experiments). We also found that the plasma membrane localization of GFP fluorescence did not change upon addition of metabolic inhibitors (2-deoxyglucose plus oligomycin) that cause cell ATP depletion, thus inhibiting exchange activity (data not shown). Furthermore, we found no changes in the plasma membrane localization of GFP-tagged CHP1 mutants EF3m and EF4m after these various treatments (data not shown). These observations suggest that CHP1 is tightly associated with NHE1 in the plasma membrane and that this interaction is not affected by various stimuli.

All the cells expressing CHP1–GFP or its mutant derivatives exhibited high Na^+/H^+ exchange activity. The $^{22}Na^+$ uptake activity in cells clamped at acidic pH$_i$ (5.6) by the K^+/nigericin technique was in the range of 20–50 nmol/mg/min (data not shown). We compared the $^{22}Na^+$ uptake activities in cells expressing various CHP1 variants in the physiological pH$_i$ range. As shown in Figure 6A, the ratio of $^{22}Na^+$ uptake at pH$_i$ 7.2–5.6 was not significantly altered by expression of wild-type CHP1. Although a previous study (*11*) indicated that overexpression of CHP1 inhibits the NHE1 activity in the presence of serum, we observed no such CHP1-induced inhibition of the exchange activity. The reason for this discrepancy is unknown. Unlike the wild-type CHP1, the $^{22}Na^+$ uptake ratio was significantly reduced by EF3 or EF4 mutants. Consistent with this finding, we observed that mutations of EF3 or EF4 significantly reduced the cytoplasmic alkalinization in response to PDGF-BB, thrombin, phorbol ester, serum, or hyperosmotic stress (sucrose) (Figure 6B). These observations suggest that mutation of EF3 or EF4 partly impairs the regulation of NHE1 by reducing pH$_i$ sensitivity. In contrast, double mutation (EF34m) of CHP1 at EF3 and EF4 did not reduce the $^{22}Na^+$ uptake ratio or cytoplasmic alkalinization (Figure 6A,B), consistent with the finding that this mutant CHP1 is not able to replace the endogenous CHP1 because of its weak interaction with NHE1. Finally, mutation of the myristoylation site (G2A) or EF1 did not affect pH$_i$-dependent regulation of NHE1.

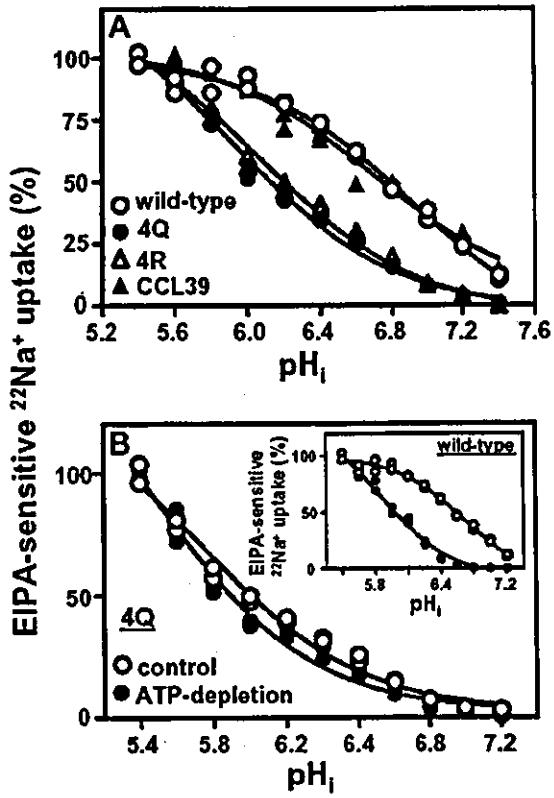

FIGURE 7: pH_i dependence of exchange activity in cells expressing some NHE variants. Panel A shows the pH_i dependence of $^{22}Na^+$ uptake in PS120 cells expressing wild-type NHE1 or CHP1 binding-defective mutants 4Q and 4R and CCL39 fibroblastic cells (the parental cell line of PS120). pH_i was clamped at various values with K^+/nigericin. The maximal EIPA-sensitive $^{22}Na^+$ uptake activity measured at $pH_i = 5.4$ was high in cells expressing wild-type NHE1 (~50 nmol/mg/min), while it was lower but similar in cells expressing 4Q or 4R or in CCL39 cells (4.2, 4.2, or 4.1 nmol/mg/min, respectively). Data were normalized according to the maximal activity at $pH_i = 5.4$. Panel B shows the effects of ATP depletion on pH_i dependence of exchange activity in cells expressing 4Q or wild-type NHE1 (inset). Cells were depleted of ATP by treatment with the metabolic inhibitors 2-deoxyglucose (5 mM) and oligomycin (2 μg/mL). Data were normalized according to the maximal activity at $pH_i = 5.4$.

Properties of NHE1 Mutants Lacking CHP1 Binding. As described above, mutations of CHP1 partly impair pH_i-dependent regulation of NHE1. Therefore, it is of interest to determine how CHP1 binding affects the pH_i sensitivity of NHE1. Previously, we described two CHP1 binding-defective mutant exchangers, 4Q or 4R, in which Phe^{526}, Leu^{527}, Leu^{530}, and Leu^{531} of NHE1 were replaced by four glutamine or arginine residues, respectively (*12*) (see Figure 4B). In this study, by using extensive H^+-killing selection, we obtained cells overexpressing 4Q or 4R and exhibiting relatively high activity (~4 nmol/mg/min at pH_i 5.4), thus allowing reliable measurement of the pH_i dependence of $^{22}Na^+$ uptake. As shown in Figure 7A, these mutations caused a marked acidic shift in the pH_i dependence (Figure 7A). As a control, we confirmed that CCL39 cells (the parental cell line of PS120) that exhibit exchange activity (V_{max}) comparable to 4Q or 4R show a pH_i dependence of exchange similar to that of PS120 cells overexpressing NHE1. In cells expressing these mutant exchangers, ATP depletion did not change the pH_i sensitivity of $^{22}Na^+$ uptake (Figure 7B). In addition, cytoplasmic alkalinization in response to extracellular stimuli, such as thrombin, PDGF-BB, hyperosmolarity, LPA, and PMA, was not observed in cells expressing 4Q or 4R (data not shown), consistent with the finding that these mutants exhibit an acidic shift of pH_i dependence.

DISCUSSION

In this study, we examined the role of CHP1, particularly its EF-hand Ca^{2+} binding motifs, in the pH_i-dependent regulation of NHE1. Our results indicated that a Ca^{2+} ion binds to each of EF3 and EF4 in CHP1 with an overall apparent K_d of ~90 nM and a Hill coefficient of ~1.0 (Table 1). This Ca^{2+} binding affinity was close to that of another family member, CaN-B (apparent $K_d \approx 70$ nM) (*36*), although the apparent K_d values for Ca^{2+} in other EF-hand Ca^{2+} binding proteins vary widely (0.01−10 μM) (*36*−*39*). Although CHP1 potentially has four Ca^{2+} binding motifs, the two ancestral sites EF1 and EF2 do not bind Ca^{2+}. This is in sharp contrast to CaN-B in which all four EF-hand motifs are able to bind Ca^{2+}, although the two N-terminal sites, EF1 and EF2, have lower affinity for Ca^{2+} than the C-terminal sites, EF3 and EF4 (*36*). Intriguingly, the Ca^{2+} affinity of CHP1 increased markedly upon complex formation with the NHE1 fragment (aa 503−545). Consistent with this finding, $^{45}Ca^{2+}$ release from the complex was much slower than that from CHP1 alone. The extraordinarily high affinity of CHP1 for Ca^{2+} (~2 nM) suggests that the CHP1/NHE1 complex always contains two Ca^{2+} ions under physiological conditions.

The high affinity for Ca^{2+} was also observed in mutant CHP1 proteins EF3m and EF4m, which have a single Ca^{2+} binding site, complexed with the NHE1 fragment. Increases in the affinity for Ca^{2+} by interaction with target proteins have also been reported for other Ca^{2+} binding proteins. For example, the Ca^{2+} binding affinity for calmodulin was increased 16- to 38-fold upon interaction with myosin light chain kinase (*40*), 2.6-fold with myristoylated alanine-rich protein kinase C substrate peptide (*41*), and 75-fold with the calmodulin binding peptide in CaN-A (*36*). CHP1 was reported to interact with other proteins, such as microtubules (*25*), CaN-A (*24*), DRAK2 (*26*), and KIF1Bβ2 (*27*), as well as members of the NHE1 family. Therefore, interaction with these proteins may also modify the Ca^{2+} binding affinity of CHP1.

Although mutation of CHP1 at either EF3 or EF4 impaired binding of 1 mol of Ca^{2+}, it did not appear to affect the interaction of CHP1 with NHE1 as shown by in vitro binding of these mutant proteins, coimmunoprecipitation, and the plasma membrane localization of GFP-tagged CHP1. Therefore, these mutations do not appear to induce marked structural distortions. However, double mutation (EF34m) at both EF3 and EF4 impaired the interaction of CHP1 with NHE1. Consistent with this finding, Ca^{2+} removal by EGTA from the wild-type CHP1 reduced the interaction with NHE1 in a pull-down assay through the amyrose resin column (data not shown). Thus, the tight association of NHE1 with CHP1 requires binding of at least one Ca^{2+} on either EF3 or EF4. Furthermore, it should be noted that the effect of double mutation (EF34m) on regulation of NHE1 cannot be properly analyzed in cells that express endogenous CHP1.

We found that expression of NHE1, but not the CHP1 binding-deficient mutant derivatives 4Q and 4R, significantly

increased the amount of endogenous CHP1. However, coexpression of GFP-tagged CHP1 proteins (wild-type, EF3m, and EF4m) preserving the strong interaction with NHE1 greatly reduced the amount of endogenous CHP1. Thus, the amount of endogenous CHP1 in cells is strongly dependent on the number of available CHP1 binding sites provided from NHE1. Although the precise reason for this is unknown, it is likely that interaction with target proteins is required for stable expression of CHP1. That is, dissociation from the target proteins may promote CHP1 degradation.

In this study, we found that CHP1 binding-defective mutants of NHE1 (4Q and 4R) caused a marked acidic shift in the pH_i dependence of Na^+/H^+ exchange activity and completely impaired ATP depletion-induced inhibition and cytoplasmic alkalinization in response to various stimuli. As we reported previously (*32*), not only mutation of the CHP1 binding region, but also deletions of different regions in the amino-terminus (subdomain I, amino acids 515−595) of the NHE1 cytoplasmic domain also markedly reduced pH_i sensitivity. Thus, subdomain I with bound CHP1 appears to be a key structure that permits the putative "pH-sensor" to maintain a physiologically relevant conformation.

We found that mutation of EF3 or EF4 in CHP1 significantly reduced the Na^+/H^+ exchange activity in the physiological neutral pH_i range and reduced the cytoplasmic alkalinization in response to various extracellular signals by decreasing the pH_i sensitivity of NHE1. Thus, mutation of each EF-hand in CHP1 somehow affects the pH_i-sensing of NHE1, although we could not evaluate the function of the double mutant CHP1 (EF34m) because of its weak interaction with NHE1. We found that EF3m, EF4m, and EF34m proteins migrated slowly on SDS−PAGE, suggesting that significant conformational changes of CHP1 occur upon mutation of each EF-hand. Such conformational changes appear to be due to removal of Ca^{2+} rather than the amino acid substitution itself, because incubation with EGTA resulted in similar slow migration of the wild-type CHP1 on SDS−PAGE (data not shown). Thus, the bound Ca^{2+} may play an important role in maintaining the CHP1 structure, thereby preserving the physiological pH_i sensitivity of NHE1.

According to the structural model of CHP1 deduced from the three-dimensional structure of CaN-B (*43*), EF-hand Ca^{2+} binding motifs would be located on the surface opposite the side where CHP1 binds to NHE1. It is likely that the surface of CHP1 with tightly bound Ca^{2+} controls the pH_i-sensing by interacting with other region(s) of NHE1. We observed that the pH_i sensitivity of NHE1 was markedly reduced by insertion of one amino acid residue (alanine) just to the N-terminal side (position aa 504 or 508) of the CHP1 binding site of NHE1, while the CHP1 binding ability was preserved (our unpublished observations). Therefore, the correct spatial orientation of CHP1 would be important for regulation of NHE. Recently, we reported that mutation of Arg^{440} in intracellular loop 5 (IL5), which connects transmembrane helices 10 and 11, markedly reduces the pH_i sensitivity of NHE1 (*44*). Thus, IL5 may interact with the CHP1 surface with tightly bound Ca^{2+}.

Many EF-hand Ca^{2+} binding proteins are known to regulate the functions of their target proteins in response to cytosolic Ca^{2+} mobilization. However, it is unlikely that CHP1 functions as such a Ca^{2+} sensor in the regulation of NHE1 because the affinity for Ca^{2+} ($K_d = \sim 2$ nM) for the CHP1/NHE1 complex differs substantially from the range of intracellular Ca^{2+} concentrations (0.1−10 μM). Instead, two EF-hand motifs of CHP1 together with tightly bound Ca^{2+} would serve as structurally important elements for preserving the normal function of NHE1, as discussed above. Such a structural role has also been suggested in the C-terminal EF-hand motifs in CaN-B (*42*) and in CaM (*41*). On the other hand, we reported previously that CaM interacts in a Ca^{2+}-dependent manner with the middle of the cytoplasmic domain of NHE1, which in the unstipulated state serves as an auto inhibitory domain decreasing the pH_i sensitivity of NHE1 (*14*, *15*). The interaction of NHE1 with CaM is strictly Ca^{2+}-dependent, although it is much weaker than that with CHP1 (*14*). Previously, we proposed that NHE1 may be activated by Ca^{2+}-dependent interaction of CaM in response to Ca^{2+}-mobilizing signals (*15*). Our previous (*14*, *15*) and several recent reports (*45*−*48*) reinforced the idea that CaM serves as an important regulatory protein in activation of NHE1 in response to hyperosmotic stress or Ca^{2+}-mobilizing agonists. NHE1 thus appears to be dually regulated by two Ca^{2+} binding proteins, CHP1 and CaM, similar to CaN-A. The former would preserve the physiological pH_i sensitivity of NHE1, whereas the latter would play a role in sensing cytosolic Ca^{2+}.

In summary, our current results suggest that the interaction of CHP1 with NHE1 is crucial for preserving the physiological pH_i sensitivity of NHE1 and that tightly bound Ca^{2+} serves as an important structural element that is required for this role. The significant effects of mutations in EF-hands on NHE1 regulation prompted us to generate a more efficient dominant negative mutant CHP1. In addition, the functional difference between CHP1 and CHP2, which we reported recently (*13*), provides important information for identification of the critical residues of CHP1. Further studies including analyses of the functions of mutated or chimerical CHP1 and determination of the crystal structure of CHP1/NHE1 complex are required to elucidate the molecular mechanism of CHP regulation of NHE1 and other NHE family members.

REFERENCES

1. Wakabayashi, S., Shigekawa, M., and Pouysségur, J. (1997) Molecular physiology of vertebrate Na^+/H^+ exchangers, *Physiol. Rev. 77*, 51−74.
2. Orlowski, J., and Grinstein, S. (1997) Na^+/H^+ exchangers of mammalian cells, *J. Biol. Chem. 272*, 22373−22376.
3. Counillon, L., and Pouysségur, J. (2000) The expanding family of eucaryotic Na^+/H^+ exchangers, *J. Biol. Chem. 275*, 1−4.
4. Sardet, C., Franchi, A., and Pouysségur, J. (1989) Molecular cloning, primary structure, and expression of the human growth factor-activatable Na^+/H^+ antiporter, *Cell 56*, 271−280.
5. Orlowski, J., Kandasamy, R. A., and Shull, G. E., (1992) Molecular cloning of putative members of the Na/H exchanger gene family, *J. Biol. Chem. 267*, 9331−9339.
6. Tsé, C.-M., Brant, S. R. Walker, M. S., Pouysségur, J., and Donowitz, M. (1992) Cloning and sequencing of a rabbit cDNA encoding and intestinal and kidney-specific Na^+/H^+ exchanger isoform (NHE-3), *J. Biol. Chem. 267*, 9340−9346.
7. Numata, M., Petrecca, K., Lake, N., and Orlowski, J. (1998) Identification of a mitochondrial Na^+/H^+ exchanger, *J. Biol. Chem. 273*, 6951−6959.
8. Numata, M., and Orlowski, J. (2001) Molecular cloning and characterization of a novel (Na^+, K^+)/H^+ exchanger localized to the *trans*-Golgi network, *J. Biol. Chem. 276*, 17387−17394.
9. Baird, N., Orlowski, J., Szabo, E. Z., Zaun, H. Schultheis, P. J., Menon, A. G., and Shull, G. (1999) Molecular cloning, genomic

organization, and functional expression of Na^+/H^+ exchanger isoform 5 (NHE5) from human brain, *J. Biol. Chem. 274*, 4377−4382.
10. Goyal, S., Vanden Heuvel, G., and Aronson, P. S. (2003) Renal expression of novel Na^+/H^+ exchanger isoform NHE8, *Am. J. Physiol. 284*, F467−473.
11. Lin, X., and Barber, D. L. (1996) A calcineurin homologous protein inhibits GTPase-stimulated Na−H exchange, *Proc. Natl. Acad. Sci. U.S.A. 93*, 12631−12636.
12. Pang, T., Su, X., Wakabayashi, S., and Shigekawa, M. (2001) Calcineurin homologous protein as an essential cofactor for Na^+/H^+ exchangers, *J. Biol. Chem. 276*, 17367−17372.
13. Pang, T., Wakabayashi, S., and Shigekawa, M. (2002) Expression of calcineuin B homologous protein 2 protects serum deprivaion-induced cell death by serum-independent activation of Na^+/H^+ exchanger, *J. Biol. Chem. 277*, 43771−43777.
14. Bertrand, B., Wakabayashi, S., Ikeda, T., Pouysségur, J., and Shigekawa, M. (1994) The Na^+/H^+ exchanger isoform 1 (NHE1) is a novel member of the calmodulin-binding proteins: Identification and characterization of calmodulin-binding sites, *J. Biol. Chem. 269*, 13703−13709.
15. Wakabayashi, S., Bertrand, B., Ikeda, T., Pouysségur, J., and Shigekawa, M. (1994) Mutation of calmodulin-binding site renders the Na^+/H^+ exchanger (NHE1) highly H^+-sensitive and Ca^{2+} regulation-defective, *J. Biol. Chem. 269*, 13710−13715.
16. Voyno-Yasenetskaya, T., Conklin, B. R., Gilbert, R. L., Hooley, R., Bourne, H. R., and Barber, D. L. (1994) G alpha 13 stimulates Na−H exchange, *J. Biol. Chem. 269*, 4721−4724.
17. Bianchini, L., L'Allemain, G., and Pouysségur, J. (1997) The p42/p44 Mitogen-activated protein kinase cascade is determinant in mediating activation of the Na^+/H^+ exchanger (NHE1 isoform) in response to growth factors, *J. Biol. Chem. 272*, 271−279.
18. Takahashi, E., Abe, J.-I., Gallis, B., Aebersold, R., Spring, D. J., Krebs, E. G., and Berk, B. C. (1999) $p90^{RSK}$ is a serum-stimulated Na^+/H^+ exchanger isoform-1 kinase. Regulatory phosphorylation of serine 703 of Na^+/H^+ exchanger isoform-1, *J. Biol. Chem. 274*, 20206−20214.
19. Lehoux, S., Abe, J. I., Florian, J. A., and Berk, B. C. (2001) 14-3-3 binding to Na^+/H^+ exchanger isoform-1 is associated with serum-dependent activation of Na^+/H^+ exchange, *J. Biol. Chem. 276*, 15794−15800.
20. Yan, W., Nehrke, K., Choi, J., and Barber, D. L. (2001) The Nck-interacting kinase (NIK) phosphorylates the Na^+-H^+ exchanger NHE1 and regulates NHE1 activation by platelet-derived growth factor, *J. Biol. Chem. 276*, 31349−31356.
21. Aharonovitz, O., Zaun, H. C., Balla, T., York, J. D., Orlowski, J., and Grinstein, S. (2000) Intracellular pH regulation by Na^+/H^+ exchange requires phosphatidylinositol 4,5-bisphosphate, *J. Cell Biol. 150*, 213−224.
22. Li, X., Alvarez, B., Casey, J. R., Reithmeier, R. A. F., and Fliegel, L. (2002) Carbionic anhydrase II binds to and enhances activity of the Na^+/H^+ exchanger, *J. Biol. Chem. 277*, 36085−36091.
23. Barroso, M. R., Bernd, K. K., DeWitt, N. D., Chang, A., Mills, K., and Sztul, E. S. (1996) A novel Ca^{2+}-binding protein, p22, is required for constitutive membrane traffic, *J. Biol. Chem. 271*, 10183−10187.
24. Lin, X., Sikkink, R. A., Rusnak, F., and Barber, D. L. (1999) Inhibition of calcineurin phosphatase activity by a calcineurin B homologous protein, *J. Biol. Chem. 274*, 36125−36131.
25. Timm, S., Titus, B., Bernd, K., and Barroso, M. (1999) The EF-hand Ca^{2+}-binding protein p22 associates with microtubules in an N-myristoylation-dependent manner, *Mol. Biol. Cell 10*, 3473−3488.
26. Matsumoto, M., Miyake, Y., Nagita, M., Inoue, H., Shitakubo, D., Takemoto, K., Ohtsuka, C., Murakami, H., Nakamura, N., and Kanazawa, H. (2001) A serine/threonine kinase which causes apoptosis-like cell death interacts with a calcineurin B-like protein capable of binding Na^+/H^+ exchanger, *J. Biochem. (Tokyo) 130*, 217−225.
27. Nakamura, N., Miyake, Y., Matsushita, M., Tanaka, S., Inoue, H., and Kanazawa, H. (2002) KIF1Bβ2, capable of interacting with CHP, is localized to synaptic vesicles, *J. Biochem. (Tokyo) 132*, 483−492.
28. Inoue, H., Nakamura, Y., Nagita, M., Takai, T., Masuda, M., Nakamura, N., and Kanazawa, H. (2003) Calcineurin homologous protein isoform 2 (CHP2). Na^+/H^+ exchangers-binding protein, is expressed in intestinal epithelium, *Biol. Pharm. Bull. 26* (2), 148−155.
29. Pouysségur, J., Sardet, C., Franchi, A., L'Allemain, G., and Paris, S. (1984) A specific mutation abolishing Na^+/H^+ antiport activity in hamster fibroblasts precludes growth at nertral and acidic pH, *Proc. Natl. Acad. Sci. U.S.A. 81*, 4833−4837.
30. Wakabayashi, S., Fafournoux, P., Sardet, C., and Pouysségur, J. (1992) The Na^+/H^+ antiporter cytoplasmic domain mediates growth factor signals and controls "H^+-sensing", *Proc. Natl. Acad. Sci. U.S.A. 89*, 2424−2428.
31. Wakabayashi, S., Ogurusu, T., and Shigekawa, M. (1986) Factors influencing calcium release from the ADP-sensitive phosphoenzyme intermediate of the sarcoplasmic reticulum ATPase, *J. Biol. Chem. 261*, 9762−9769.
32. Ikeda, T., Schmitt, B., Pouysségur, J., Wakabayashi, S., and Shigekawa, M. (1997) Identification of cytoplasmic subdomains that control pH-sensing of theNa^+/H^+ exchanger (NHE1): pH-maintenance, ATP-sensitive, and flexible loop domains, *J. Biochem. (Tokyo) 121*, 295−303.
33. Strynadka, N. C. J., and James, M. N. G. (1989) Crystal structures of the helix-loop-helix calcium-binding proteins, *Annu. Rev. Biochem. 58*, 951−998.
34. Yap, K. L., Ames, J. B., Swindells, M. B., and Ikura, M. (1999) Diversity of conformational states and changes within the EF-hand protein superfamily, *Proteins 37*, 499−507.
35. Szebenyi, D. M. E., Obendorf, S. K., and Moffat, K. (1981) Structure of vitamin D-dependent calcium-binding protein from bovine intestine, *Nature 294*, 327−332.
36. Stemmer, P. M., and Klee, C. B. (1994) Dual Calcium Ion Regulation of Calcineurin by Calmodulin and Calcineurin B, *Biochemistry 33*, 6859−6866.
37. Pauls, T. L., Durussel, I., Cox, J. A., Clark, I. D., Szabo, A. G., Gagne, S. M., Sykes, B. D., and Berchtold, M. W. (1993) Metal binding properties of recombinant rat parvalbumin wild-type and F102W mutant, *J. Biol. Chem. 268*, 20897−20903.
38. Gross, M. D., Gosnell, M., Tsarbopoulos, A., and Hunziker, W. (1993) A functional and degenerate pair of EF hands contains the very high affinity calcium-binding site of calbindin-D_{28K}, *J. Biol. Chem. 268*, 20917−20992.
39. Burgoyne, R. D., and Weiss, J. L. (2001) The neuronal calcium sensor family of Ca^{2+}-binding proteins, *Biochem. J. 353*, 1−12.
40. Olwin, B. B., Edelman, A. M., Krebs, E. G., and Storm, D. R. (1984) Quantitation of energy coupling between Ca^{2+}, calmodulin, skeletal muscle myosin light chain kinase, and kinase substrates, *J. Biol. Chem. 259*, 10949−10955.
41. Johnson, J. D., Snyder, C., Walsh, M., and Flynn, M. (1996) Effects of myosin light chain kinase and peptides on Ca^{2+} exchange with the N- and C-terminal Ca^{2+} binding sites of calmodulin, *J. Biol. Chem. 271*, 761−767.
42. Feng, B., and Stemmer, P. M. (1999) Interactions of calcineurin A, calcineurin B, and Ca^{2+}, *J. Biol. Chem. 38*, 12481−12489.
43. Kissinger, C. R., Parge, H. E., Knighton, D. R., Lewis, C. T., Pelletier, L. A., Tempczyk, A., Kalish, V. J., Tucker, K. D., Showalter, R. E., Moomaw, E. W., Gastinel, L. N., Habuka, N., Chen, X., Maldonado, F., Barker, J. E., Bacquet, R., and Villafranca, J. E. (1995) Crystal structures of human calcineurin and the human FKBP12−FK506-calcineurin complex, *Nature 378*, 641−644.
44. Wakabayashi, S., Hisamitsu, T., Pang, T., and Shigekawa, M. (2003) Mutations of Arg^{440} and Gly^{455}/Gly^{456} oppositely change pH sensing of Na^+/H^+ exchanger 1, *J. Biol. Chem. 278*, 11828−11835.
45. Garnovaskaya, M. N., Mukhin, Y. V., Vlasova, T. M., and Raymond, J. R. (2003) Hypertonicity activates Na^+/H^+ exchange through Janus kinase 2 and calmodulin, *J. Biol. Chem. 278*, 16908−16915.
46. Mukhin, Y. V., Vlasova, T., Jaffa, A. A., Collinsworth, G., Bell, J. L., Tholanikunnel, B. G., Petus, T., Fitzgibbon, W., Ploth, D. W., Raymond, J. R., and Garnovskaya, M. N. (2001) Bradykinin B_2 receptors activate Na^+/H^+ exchange in mIMCD-3 cells via Janus kinase 2 and Ca^{2+}/calmodulin, *J. Biol. Chem. 276*, 17339−17346.
47. Robertson, M. A., Woodside, M., Foskett, J. K., Orlowski, J., and Grinstein, S. (1997) Muscarinic agonists induce phosphorylation-independent activation of the NHE−1 isoform of the Na^+/H^+ antiporter in salivary acinar cells, *J. Biol. Chem. 272*, 287−294.
48. Moor, AN, Murtazina, R, and Fliegel, L. (2000) Calcium and osmotic regulation of the Na^+/H^+ exchanger in neonatal ventricular myocytes, *J. Mol. Cell. Cardiol. 32*, 925−936.

BI0360004

ELSEVIER

Autonomic Neuroscience: Basic and Clinical 111 (2004) 140–143

AUTONOMIC NEUROSCIENCE: *Basic & Clinical*

www.elsevier.com/locate/autneu

Short communication

In vivo assessment of catechol *O*-methyltransferase activity in rabbit skeletal muscle

Takafumi Fujii[a], Toji Yamazaki[a,*], Tsuyoshi Akiyama[a], Shunji Sano[b], Hidezo Mori[a]

[a] *Department of Cardiac Physiology, National Cardiovascular Center Research Institute, 5-7-1, Fujishirodai, Suita, Osaka 565-8565, Japan*
[b] *Department of Cardiovascular Surgery, Okayama University Medical School, Okayama 700-8558, Japan*

Received 25 December 2003; received in revised form 23 January 2004; accepted 9 February 2004

Abstract

With the use of microdialysis technique in the anesthetized rabbit, we examined the catechol *O*-methyltransferase (COMT) activity at the skeletal muscle interstitium. We implanted a dialysis probe into the adductor muscle, and monitored dialysate catecholamines and their metabolites with chromatogram-electrochemical detection. Administration of COMT inhibitor (entacapone) decreased dialysate 3-methoxy 4-hydroxyphenylglycol (MHPG) levels. Local administration of dihydroxyphenylglycol induced increases in dialysate MHPG levels. These increases in dialysate MHPG levels were suppressed by the addition of entacapone. The concentration of MHPG in the skeletal muscle dialysate corresponded to the COMT activity in the skeletal muscle. Furthermore, local administration of norepinephrine or epinephrine increased normetanephrine or metanephrine levels in dialysate but not MHPG levels. Skeletal muscle microdialysis with local administration of catecholamine offers a new method for in vivo assessment of regional COMT activity.

Keywords: Catecholamine; Catechol *O*-methyltransferase; Entacapone; Microdialysis; Skeletal muscle

Catechol *O*-methyltransferase (COMT) exerts a critical action on the inactivation of catecholamrines and catecholestrogens (Boulton and Eisenhofer, 1998). COMT enzyme exists in almost all mammalian tissues and organs (Karhunen et al., 1994; Männistö and Kaakkola, 1999). The wide distribution of COMT in different tissues suggests an important physiological role for COMT activity. In vitro COMT activity has been widely assessed in various tissues (Männistö and Kaakkola, 1999; Tsunoda et al., 2002), while in vivo COMT activity has been assessed only in erythrocyte (Toumainen et al., 1996). To determine whether COMT activity is involved in cardiovascular regulation, we need information about in vivo COMT activity in organs and tissues.

A sophisticated technique using radiotracers has been employed for spillover of organ specific metabolite formed by COMT activity (3-methoxy 4-hydroxyphenylglycol, MHPG) (Lambert et al., 1995). This study suggested that majority of MHPG in plasma was derived from skeletal muscle, with the exception of central nervous system. Dispersed organs, such as skeletal muscle, have a thin and diffuse sympathetic innervation, but skeletal muscle is one candidate suitable for investigating regional MHPG production (Tokunaga et al., 2003a,b). This organ is suited to microdialysis probe implantation. Recently we have developed the skeletal muscle microdialysis for the monitoring of catecholamines and their metabolites. At the skeletal muscle, the small amounts of dialysate norepinephrine and its metabolites could be determined by microdialysis with electrochemical detection.

In the present study, we examined whether COMT blocker affected regional norepinephrine kinetics at the skeletal muscle interstitial spaces. With the use of dialysis technique, the dialysate was sampled from the skeletal muscle, and dialysate catecholamines and their metabolites levels were measured with liquid chromatography. Further, the study was designed to examine regional *O*-methylation products evoked by local administration of catecholamine and determine whether these data provide information about in vivo regional COMT activity.

Male Japanese white rabbits weighing 2.6–3.1 kg each were anesthetized with pentobarbital sodium (30–35 mg/kg,

* Corresponding author. Tel.: +81-6-6833-5012; fax: +81-6-6872-8092.
E-mail address: yamazaki@ri.ncvc.go.jp (T. Yamazaki).

1566-0702/$ - see front matter © 2004 Elsevier B.V. All rights reserved.
doi:10.1016/j.autneu.2004.02.001

i.v.). The level of anesthesia was maintained with a continuous intravenous infusion of pentobarbital sodium (1–2 mg/kg/h). After tracheotomy, the animals were ventilated with room air mixed with oxygen. Body temperature was maintained with a heated pad and lamp. All protocols were performed in accordance with the American Physiological Society guidelines for the use of animals. After a longitudinal skin incision was made in the left groin, the dialysis probes were implanted in the left adductor muscle with a fine guiding needle.

For skeletal muscle dialysis, we designed a transverse dialysis probe. The dialysis fiber (13 mm length, 0.31 mm O.D. and 0.2 mm I.D.; PAN-1200, 50,000 molecular mass cutoff, Asahi Chemical, Tokyo, Japan) was glued at both ends into a polyethylene tube (25 cm length, 0.5 mm O.D. and 0.2 mm I.D.) (Akiyama et al., 1991; Tokunaga et al., 2003a,b). The dialysis probe was perfused with Ringer solution at a speed of 10 μl/min using a microinjection pump (CMA 102, Carnegie Medicin, Stockholm, Sweden). Dialysate catecholamines and their metabolite concentrations were measured by high-performance liquid chromatography with electrochemical detection (Takauchi et al., 1997; Tokunaga et al., 2003a,b; Yamazaki et al., 1995).

Basal dialysate norepinephrine, dihydroxyphenylglycol (DHPG) and MHPG levels were presented in Table 1. Entacapone (COMT blocker) was intraperitoneally administered (10 mg/kg) (Illi et al., 1995; Scheinin et al., 1998). Administration of entacapone decreased the MHPG level of dialysate but increased the DHPG levels of dialysate. The dialysate norepinephrine levels were not affected by entacapone. These changes were preserved 2 h after administration of entacapone.

To examine regional COMT activity, we measured the formation of MHPG evoked by local administration of exogenous DHPG via dialysis probe. We determined doses of DHPG based on the dialysate DHPG concentration in the previous experiments (Akiyama and Yamazaki, 2001). Local administration of DHPG (25, 250 ng/ml) dose-dependently increased the MHPG levels of dialysate (Fig. 1). These increases in the MHPG levels were prevented by pretreatment with entacapone.

In this study, exogenous DHPG dose-dependently increased the MHPG levels of dialysate. Exogenous DHPG via the dialysis probe easily traversed the cell membrane and reached skeletal muscle (Goldstein et al., 1998). In contrast, entacapone significantly decreased the MHPG levels of

Table 1
Basal dialysate NE, DHPG, and MHPG levels in rabbit skeletal muscle

	Before entacapone	After entacapone
NE (pg/ml)	8±1	10±1
DHPG (pg/ml)	27±4	53±11*
MHPG (pg/ml)	198±12	147±18*

NE, norepinephrine; DHPG, dihydroxyphenylglycol; MHPG, 3-methoxy 4-hydroxyphenylglycol. Values are means±SE. n=5.
* P<0.05 vs. values before entacapone.

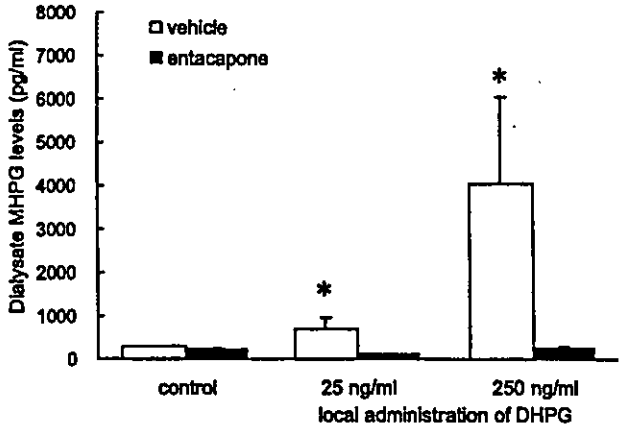

Fig. 1. Effects of exogenous dihydroxyphenylglycol (DHPG) infusion on the 3-methoxy 4-hydroxyphenylglycol (MHPG) production. Local administration of DHPG dose-dependently increased the MHPG levels of dialysate. These increases in the MHPG levels were prevented by pretreatment with entacapone. Values are means±SE (n=5). *P<0.05 vs. control.

dialysate. These data suggest that regional COMT activity corresponds to the production of dialysate MHPG levels. Furthermore, entacapone induced a decrease in the dialysate MHPG level accompanied by an increase in the dialysate DHPG but not norepinephrine level. Therefore we consider that regional DHPG is one possible substrate for MHPG production, and that the concentration of MHPG or MHPG/DHPG ratio in the skeletal muscle dialysate might correspond to the COMT activity in the skeletal muscle.

Earlier studies suggested species and organ differences in extraneuronal uptake and COMT activity (Scheinin et al., 1998; Tsunoda et al., 2002). Extraneuronal norepinephrine uptake and COMT activity were well examined in rabbit heart with the findings suggesting that rabbit heart hardly metabolizes isoprenaline to methoxyprenaline (Lindmar and Löffelholz, 1974). Thus rabbit heart seems to have a very poorly developed extraneuronal system, including weak COMT activity, for the uptake and metabolism of catecholamines (Trendelenburg, 1978). On the other hand, rabbit aortic strips have a high capacity for COMT activity (Levin, 1974). From these and previous data (Tokunaga et al., 2003a,b), the ratio of MHPG/DHPG in myocardium and skeletal muscle were 1.0±0.2 and 7.9±1.3, respectively. Rabbit skeletal muscle seems to have a well-developed COMT activity. In the skeletal muscle sympathetic innervation was not dense, and the DHPG levels were less than that of heart (Tokunaga et al., 2003a,b). Therefore, other compounds or plasma DHPG might be involved in the regional formation of MHPG in the skeletal muscle.

MHPG is produced by extraneuronal *O*-methylation of DHPG formed intraneuronally from norepinephrine or by the extraneuronal combination of COMT and monoamine oxidase (MAO) on norepinephrine and epinephrine (Akiyama and Yamazaki, 2001; Eisenhofer et al., 1988). Therefore, MHPG is mainly yielded from DHPG, norepinephrine or epinephrine at the skeletal muscle. Furthermore,

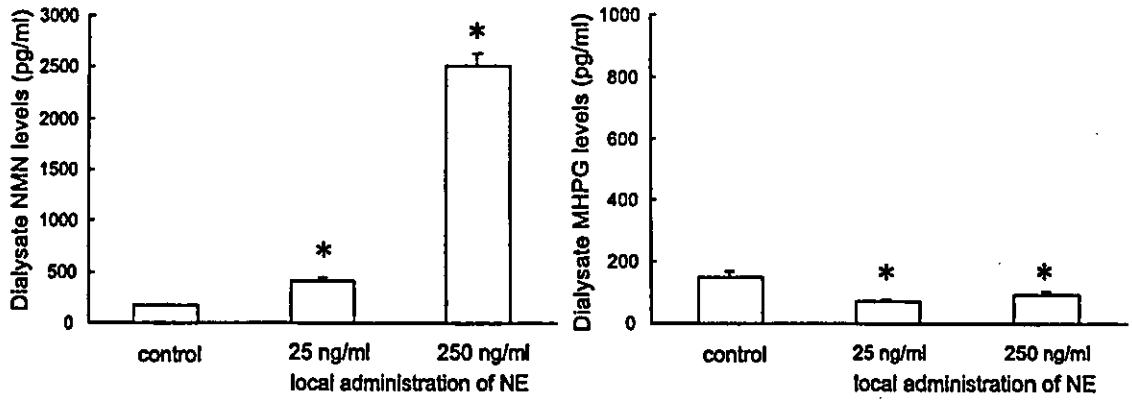

Fig. 2. Effects of exogenous norepinephrine (NE) infusion on the 3-methoxy 4-hydroxyphenylglycol (MHPG) and normetanephrine (NMN) production. Local administration of NE dose-dependently increased the NMN levels of dialysate but not MHPG levels. Values are means±SE (n=5). *P<0.05 vs. control.

O-methylation of catechol compounds includes MHPG, normetanephrine and metanephrine. We examined the relation between catecholamines and their metabolites. To compare norepinephrine and epinephrine with DHPG infusion, norepinephrine or epinephrine infusion with similar doses of DHPG was administered. Local administration of norepinephrine increased the normetanephrine levels of dialysate but not the MHPG levels (Fig. 2). Local administration of epinephrine increased the metanephrine levels of dialysate but not the MHPG levels (Fig. 3). Our data suggest that only DHPG is a possible substrate for MHPG production. Local administration of norepinephrine or epinephrine produced normetanephrine or metanephrine but not MHPG. Or rather, norepinephrine or epinephrine caused a decrease in the dialysate MHPG level. These data are consistent with data on the origins of plasma MHPG in rats, which indicated that most MHPG arises from *O*-methylation of the DHPG by intraneuronal deamination of norepinephrine (Eisenhofer et al., 1994).

Our data indicate that COMT exerts an important role on the degradation of cathecholamines in the skeletal muscular interstitium. Muscular catecholamines derive from circulating blood and surrounding sympathetic nerve systems (Tokunaga et al., 2003a,b). Therefore, COMT activity in the skeletal muscle may be related to regional or systemic sympathetic nerve activity. The relationship between regional COMT activity and sympathetic nerve activity remains to be further examined. Muscle sympathetic nerve activity is involved in the regulation of vascular tone and glucose metabolism in the skeletal muscle (Lundvall and Edfeldt, 1994; Spraul et al., 1994). Further studies concerning the physiological role of regional COMT activity on vascular or metabolic control are warranted.

To our knowledge, this is the first report on the in vivo assessment of COMT activity by direct measurement of dialysate MHPG, normetanephrine, and metanephrine obtained from skeletal muscle. Local administration of DHPG increased the MHPG levels of dialysate. These increases in MHPG were prevented by pretreatment with a COMT inhibitor. Therefore we consider that the concentration of MHPG in the skeletal muscle dialysate might correspond to the COMT activity in the skeletal muscle. Measurement of MHPG/DHPG ratio or MHPG formation evoked by DHPG infusion in skeletal muscle may be particularly appropriate for providing information about regional COMT activity. Thus skeletal muscle microdialysis with local administration of catecholamine offers a new method for in vivo assessment of regional COMT activity.

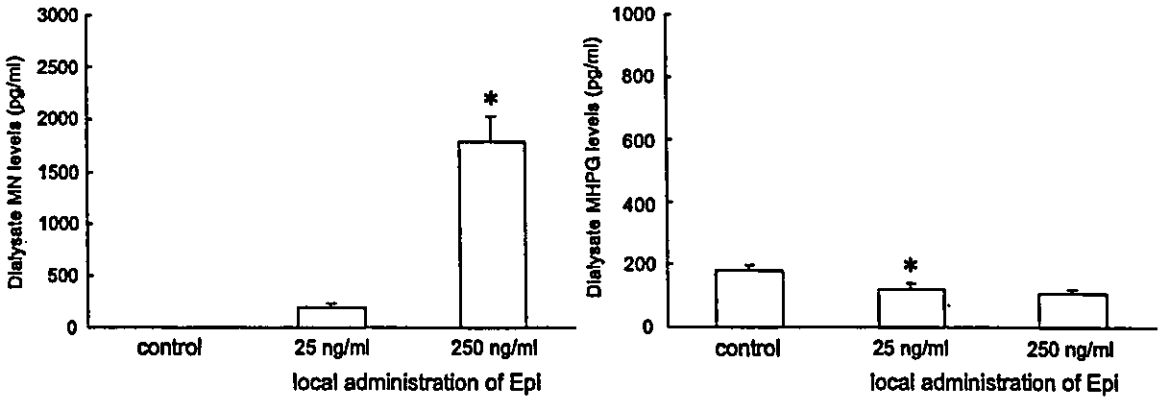

Fig. 3. Effects of exogenous epinephrine (Epi) infusion on the metanephrine (MN) and 3-methoxy 4-hydroxyphenylglycol (MHPG) production. Local administration of Epi increased the MN levels of dialysate but not MHPG levels. Values are means±SE (n=5). *P<0.05 vs. control.

Acknowledgements

This work was supported by Grants-in-Aid for scientific research (15590787) from the Ministry of Education, Culture, Sports, Science and Technology; the Research Grants for Cardiovascular Disease (H13C-1) from the Ministry of Health, Labor and Welfare. The authors thank Orion Pharma, Finland for the supply of entacapone.

References

Akiyama, T., Yamazaki, T., 2001. Myocardial interstitial norepinephrine and dihydroxyphenylglycol levels during ischemia and reperfusion. Cardiovasc. Res. 49, 78–85.

Akiyama, T., Yamazaki, T., Ninomiya, I., 1991. In vivo monitoring of myocardial interstitial norepinephrine by dialysis techniques. Am. J. Physiol. 261, H1643–H1647.

Boulton, A.A., Eisenhofer, G., 1998. Catecholamine metabolism: from molecular understanding to clinical diagnosis and treatment. Adv. Pharmacol. 42, 273–292.

Eisenhofer, G., Goldstein, D.S., Ropchak, T.G., Nguyen, H.Q., Keiser, H.R., Kopin, I.J., 1988. Source and physiological significance of plasma 3,4-dihydroxyphenylglycol and 3-methoxy-4-hydroxyphenylglycol. J. Auton. Nerv. Syst. 24, 1–14.

Eisenhofer, G., Pecorella, W., Pacak, K., Hooper, D., Kopin, I.J., Goldstein, D.S., 1994. The neuronal and extraneuronal origins of plasma 3-methoxy-4hydroxyphenylglycol in rats. J. Auton. Nerv. Syst. 50, 93–107.

Goldstein, D.S., Eisenhofer, G., Stull, R., Folio, C.J., Keiser, H.R., Kopin, I.J., 1998. Plasma dihydroxyphenylglycol and the intraneuronal disposition of norepinephrine in humans. J. Clin. Invest. 81, 213–220.

Illi, A., Sundberg, S., Ojala-Karlsson, P., Korhonen, P., Scheinin, M., Gordin, A., 1995. The effect of entacapone on the disposition and hemodynamic effects of intravenous isoproterenol and epinephrine. Clin. Pharmacol. Ther. 58, 221–227.

Karhunen, T., Tilgmann, C., Ulmanen, I., Julkunen, I., Panula, P., 1994. Distribution of catechol-*O*-methyltransferase enzyme in rat tissues. J. Histochem. Cytochem. 42, 1079–1090.

Lambert, G.W., Kaye, D.M., Vaz, M., Cox, H.S., Turner, A.G., Jennings, G.L., Esler, M.D., 1995. Regional origins of 3-methoxy-4-hydroxyphenylglycol in plasma: effects of chronic sympathetic nervous activation and denervation, and acute reflex sympathetic stimulation. J. Auton. Nerv. Syst. 55, 169–178.

Levin, J.A., 1974. The uptake and metabolism of ^{3}H-L- and ^{3}H-DL-norepinephrine by intact rabbit aorta and by isolated adventitia and media. J. Pharmacol. Exp. Ther. 190, 210–226.

Lindmar, R., Löffelholz, K., 1974. Neuronal and extraneuronal uptake and efflux of catecholamines in the isolated heart. Naunyn-Schmiedeberg's Arch. Pharmacol. 284, 63–92.

Lundvall, J., Edfeldt, H., 1994. Very large range of baroreflex sympathetic control of vascular resistance in human skeletal muscle and skin. J. Appl. Physiol. 76, 204–211.

Männistö, P.T., Kaakkola, S., 1999. Catechol-*O*-metyltransferase (COMT) activity: biochemistry, molecular biology, pharmacology, and clinical efficacy of the new selective COMT inhibitors. Pharmacol. Rev. 51, 593–628.

Scheinin, M., Illi, A., Koulu, M., Ojara-Karsson, P., 1998. Norepinephrine metabolites in plasma as indicators of pharmacological inhibition of monoamine oxidase and catechol *O*-methyltransferase. Adv. Pharmacol. 42, 367–370.

Spraul, M., Anderson, E.A., Bogardus, C., Ravussin, E., 1994. Muscle sympathetic nerve activity in response to glucose ingestion. Impact of plasma insulin and body fat. Diabetes 43, 191–196.

Takauchi, Y., Kitagawa, H., Kawada, T., Akiyama, T., Yamazaki, T., 1997. High-performance liquid chromatographic determination of myocardial interstitial dihydroxyphenylglycol. J. Chromatogr., B, Biomed. Sci. Appl. 693, 218–221.

Tokunaga, N., Yamazaki, T., Akiyama, T., Sano, S., Mori, H., 2003. In vivo monitoring of norepinephrine and its metabolites in skeletal muscle. Neurochem. Int. 43, 573–580.

Tokunaga, N., Yamazaki, T., Akiyama, T., Mori, H., 2003. Detection of 3-methoxy-4-hydroxyphenylglycol in rabbit skeletal muscle microdialysate. J. Chromatogr., B, Biomed. Sci. Appl. 798, 163–166.

Toumainen, P., Reenila, I., Männistö, P.T., 1996. Validation of assay of catechol-*O*-methyltransferase activity in human erythrocytes. J. Pharm. Biomed. Anal. 14, 515–523.

Trendelenburg, U., 1978. The extraneuronal uptake and metablosim of catecholamines in the heart. In: Paton, D.M. (Ed.), The Mechanism of Neuronal and Extranneuronal Transport of Catecholamines. Raven Press, New York, pp. 259–280.

Tsunoda, M., Takezawa, K., Masuda, M., Imai, K., 2002. Rat liver and kidney catechol-*O*-methyltransferase activity measured by high-performance liquid chromatography with fluorescence detection. Biomed. Chromatogr. 16, 536–541.

Yamazaki, T., Akiyama, T., Shindo, T., 1995. Routine high-performance liquid chromatographic determination of myocardial interstitial norepinephrine. J. chromatogr., B, Biomed. Sci. Appl. 670, 328–331.

Am J Physiol Regul Integr Comp Physiol 287: R161–R166, 2004.
First published March 18, 2004; 10.1152/ajpregu.00609.2003.

Effects of Ca^{2+} channel antagonists on acetylcholine and catecholamine releases in the in vivo rat adrenal medulla

Tsuyoshi Akiyama,[1] Toji Yamazaki,[1] Hidezo Mori,[1] and Kenji Sunagawa[2]

[1]*Department of Cardiac Physiology and* [2]*Department of Cardiovascular Dynamics, National Cardiovascular Center Research Institute, Suita, Osaka 565–8565, Japan*

Submitted 20 October 2003; accepted in final form 13 March 2004

Akiyama, Tsuyoshi, Toji Yamazaki, Hidezo Mori, and Kenji Sunagawa. Effects of Ca^{2+} channel antagonists on acetylcholine and catecholamine releases in the in vivo rat adrenal medulla. *Am J Physiol Regul Integr Comp Physiol* 287: R161–R166, 2004. First published March 18, 2004; 10.1152/ajpregu.00609.2003.—To elucidate the types of voltage-dependent Ca^{2+} channels controlling ACh and catecholamine releases in the in vivo adrenal medulla, we implanted microdialysis probes in the left adrenal medulla of anesthetized rats and investigated the effects of Ca^{2+} channel antagonists on ACh, norepinephrine, and epinephrine releases induced by nerve stimulation. The dialysis probes were perfused with Ringer solution containing a cholinesterase inhibitor, neostigmine. The left splanchnic nerves were electrically stimulated at 2 and 4 Hz before and after intravenous administration of Ca^{2+} channel antagonists. ω-Conotoxin GVIA (an N-type Ca^{2+} channel antagonist, 10 μg/kg) inhibited ACh release at 2 and 4 Hz by ~40%, norepinephrine release at 4 Hz by ~50%, and epinephrine release at 2 and 4 Hz by ~45%. A fivefold higher dose of ω-conotoxin GVIA (50 μg/kg) did not further inhibit these releases. ω-Conotoxin MVIIC (a P/Q-type Ca^{2+} channel antagonist, 50 μg/kg) inhibited ACh and epinephrine releases at 4 Hz by ~30%. Combined ω-conotoxin GVIA (50 μg/kg) and MVIIC (250 μg/kg) inhibited ACh release at 2 and 4 Hz by ~70% and norepinephrine and epinephrine releases at 2 and 4 Hz by ~80%. Nifedipine (an L-type Ca^{2+} channel antagonist, 300 and 900 μg/kg) did not change ACh release at 2 and 4 Hz; however, nifedipine (300 μg/kg) inhibited epinephrine release at 4 Hz by 20%, and nifedipine (900 μg/kg) inhibited norepinephrine and epinephrine releases at 4 Hz by 30%. In conclusion, both N- and P/Q-type Ca^{2+} channels control ACh release on preganglionic splanchnic nerve endings while L-type Ca^{2+} channels do not. L-type Ca^{2+} channels are involved in norepinephrine and epinephrine releases on chromaffin cells.

anesthetized rats; microdialysis; norepinephrine; epinephrine; preganglionic autonomic nerve endings

Ca^{2+} influx through the voltage-dependent Ca^{2+} channels induces the release of transmitters from neuronal or secretory cells by initiating exocytosis from vesicles. Voltage-dependent Ca^{2+} channels have been classified into L-, N-, P-, Q-, R-, and T-types (12, 25, 30). To better understand the mechanism controlling the release of transmitters, it is important to determine the type of Ca^{2+} channels involved in the release of the transmitters on neuronal or secretory cells.

In the in vivo adrenal medulla, catecholamine release is controlled by central sympathetic neurons through preganglionic splanchnic nerves. Splanchnic nerve endings make synaptic-like contacts with chromaffin cells (9). ACh released from splanchnic nerve endings consequently evokes catecholamine release from chromaffin cells by activation of cholinergic receptors. Thus, in vivo catecholamine release requires Ca^{2+} influx through the voltage-dependent Ca^{2+} channels at two different sites in the adrenal medulla: splanchnic nerve endings and chromaffin cells. Numerous studies have investigated the nature of Ca^{2+} channels controlling transmitter release from postganglionic autonomic nerve endings (8, 11, 32, 33, 36, 37). Little information is, however, available on the type of Ca^{2+} channels controlling the ACh release from preganglionic autonomic nerve endings including splanchnic nerve endings. Moreover, although the types of Ca^{2+} channels controlling catecholamine release have been investigated using isolated chromaffin cells in various species (5, 6, 13, 16, 21, 23, 24), it remains unknown whether endogenous ACh induces Ca^{2+} influx through the same types of Ca^{2+} channels on chromaffin cells.

We have recently developed a dialysis technique to simultaneously monitor ACh and catecholamine releases in the in vivo adrenal medulla (2). This method makes it possible to characterize Ca^{2+} channels controlling ACh release from splanchnic nerve endings and catecholamine release from adrenal medulla in the in vivo state. In the present study, we applied the microdialysis technique to the adrenal medulla of anesthetized rats and investigated the effects of Ca^{2+} channel antagonists on dialysate ACh and catecholamine responses induced by the electrical stimulation of splanchnic nerves.

MATERIALS AND METHODS

Animal preparation. The investigation conforms with the *Guide for the Care and Use of Laboratory Animals* published by the National Institutes of Health (NIH Publication No. 85–23, revised 1996). Adult male Wistar rats weighing 380–450 g were anesthetized with pentobarbital sodium (50–55 mg/kg ip). A cervical midline incision was made to expose the trachea, which was then cannulated. The rats were ventilated with a constant-volume respirator using room air mixed with oxygen. The left femoral artery and vein were cannulated for monitoring arterial blood pressure and administration of anesthetic, respectively. The level of anesthesia was maintained with a continuous intravenous infusion of pentobarbital sodium (15–25 $mg \cdot kg^{-1} \cdot h^{-1}$ iv). Electrocardiogram was monitored for recording heart rate. A thermostatic heating pad was used to keep the esophageal temperature within a range of 37–38°C. With the animal in the lateral position, the left adrenal gland and left splanchnic nerve were exposed by a subcostal flank incision, and the left splanchnic nerve was transected. Shielded bipolar stainless steel electrodes were applied to the distal end of the nerve, which was then stimulated with a digital stimulator (SEN-7203, Nihon Kohden) with a rectangular pulse (10 V and 1 ms in duration).

Address for reprint requests and other correspondence: T. Akiyama, Dept. of Cardiac Physiology, National Cardiovascular Center Research Institute, 5–7-1 Fujishiro-dai, Suita, Osaka, 565–8565 Japan (E-mail: takiyama@ri.ncvc.go.jp).

The costs of publication of this article were defrayed in part by the payment of page charges. The article must therefore be hereby marked "*advertisement*" in accordance with 18 U.S.C. Section 1734 solely to indicate this fact.

Dialysis technique. The materials of the dialysis probe were the same as those used in our previous dialysis experiments (1, 2). Briefly, each end of the dialysis fiber (0.31 mm OD, and 0.20 mm ID; PAN-1200 50,000 mol wt cutoff, Asahi Chemical) was inserted into the polyethylene tube (25-cm length, 0.5 mm OD, and 0.2 mm ID; SP-8) and glued. The length of the dialysis fiber exposed was 3 mm.

The left adrenal gland was gently lifted, and the dialysis probe was implanted in the medulla of the left adrenal gland along the long axis by using a fine guiding needle. The dialysis probe was perfused with Ringer solution containing a cholinesterase inhibitor, neostigmine (10 μM), at a speed of 10 μl/min using a microinjection pump (CMA/100, Carnegie Medicin). Ringer solution with no buffer consisted of (in mM) 147.0 NaCl, 4.0 KCl, and 2.25 $CaCl_2$. One sampling period was 2 min (1 sample volume = 20 μl). We started the protocols followed by a stabilization period of 3–4 h and sampled dialysate taking the dead space volume into account.

Dialysate ACh, norepinephrine (NE), and epinephrine (Epi) concentrations were measured as indexes of ACh and catecholamine releases in the adrenal medulla. Half of the dialysate sample was used for the measurement of ACh, and the remaining half for the measurement of NE and Epi. ACh and catecholamine assays were separately conducted using each high-performance liquid chromatography with electrochemical detection as previously described (3, 4).

Experimental design. The experiment was performed based on the previous experiment showing that dialysate ACh and catecholamine responses were reproducible on repetition of stimulation (2). The left splanchnic nerves were electrically stimulated for 2 min at 30-min intervals. Three dialysate samples were continuously collected per electrical stimulation: one before, one during, and one after stimulation. Stimulations at two different frequencies (2 and 4 Hz) were performed before and after intravenous administration of Ca^{2+} channel antagonists.

We tested three types of Ca^{2+} channel antagonists (25): the N-type Ca^{2+} channel antagonist ω-conotoxin GVIA, the P/Q-type Ca^{2+} channel antagonist ω-conotoxin MVIIC, and the L-type Ca^{2+} channel antagonist nifedipine. We determined the first doses of Ca^{2+} channel antagonists based on the dose used in the earlier experiments (7, 14, 26, 29, 37) and tested ω-conotoxin GVIA (10 μg/kg) in six rats, ω-conotoxin MVIIC (50 μg/kg) in six rats, and nifedipine (300 μg/kg) in six rats. Second, we tested a fivefold higher dose of ω-conotoxin GVIA (50 μg/kg) in six rats, a combination of fivefold higher doses of ω-conotoxin GVIA (50 μg/kg) and MVIIC (250 μg/kg) in six rats, and a threefold higher dose of nifedipine (900 μg/kg) in six rats. We did not test a higher dose of ω-conotoxin MVIIC singly because a high dose of ω-conotoxin MVIIC loses its selectivity for P/Q-type and inhibits N-type Ca^{2+} channels (18).

Nifedipine was administered twice before 2- and 4-Hz stimulation, but ω-conotoxin GVIA and MVIIC were administered once before 2-Hz stimulation because the ω-conotoxin family has long-lasting blocking actions (8, 18, 36). We assessed the responses to nerve stimulation 30, 20, and 10 min after administration of ω-conotoxin GVIA, ω-conotoxin MVIIC, and nifedipine, respectively, when heart rate and arterial pressure had already been stabilized.

At the end of the experiment the rats were killed with pentobarbital sodium, and the implant sites were examined. The dialysis probes were confirmed to have been implanted in the adrenal medulla, and no bleeding or necrosis was found macroscopically.

Drugs. Drugs were mixed fresh for each experiment. Neostigmine methylsulfate (Shionogi), ω-conotoxin GVIA (Peptide Institute), and ω-conotoxin MVIIC (Peptide Institute) were dissolved and diluted in Ringer solution. Nifedipine (Sigma Chemical) was dissolved in ethanol and diluted in Ringer solution.

Statistical methods. To examine the effects of nerve stimulation and Ca^{2+} channel antagonists, we analyzed heart rate and mean arterial pressure and dialysate ACh, NE, and Epi responses by using one-way ANOVA with repeated measures. When statistical significance was detected, the Newman-Keuls test was applied (35). Statistical significance was defined as $P < 0.05$. Values are presented as means ± SE.

RESULTS

Effects of Ca^{2+} channel antagonists on heart rate and mean arterial pressure. ω-Conotoxin GVIA (10 μg/kg) decreased heart rate from 418 ± 9 to 328 ± 13 beats/min ($P < 0.05$) and mean arterial pressure from 115 ± 2 to 74 ± 2 mmHg ($P < 0.05$). ω-Conotoxin GVIA (50 μg/kg) did not further decrease heart rate and mean arterial pressure. ω-Conotoxin MVIIC decreased heart rate from 408 ± 3 to 390 ± 5 beats/min ($P < 0.05$) but did not change mean arterial pressure. Combined ω-conotoxin GVIA and MVIIC decreased heart rate from 415 ± 10 to 327 ± 4 beats/min ($P < 0.05$) and mean arterial pressure from 124 ± 2 to 57 ± 2 mmHg ($P < 0.05$). Nifedipine (300 μg/kg) decreased mean arterial pressure from 113 ± 4 to 86 ± 4 mmHg ($P < 0.05$) but did not change heart rate. Nifedipine (900 μg/kg) decreased mean arterial pressure from 124 ± 3 to 73 ± 2 mmHg ($P < 0.05$).

Effects of Ca^{2+} channel antagonists on ACh and catecholamine releases. ACh could not be detected in dialysate before or after stimulation. Thus we expressed dialysate ACh concentration during stimulation as an index of ACh release induced by stimulation. In contrast, substantial amounts of NE and Epi were observed in dialysate before stimulation. Intravenous administration of Ca^{2+} channel antagonists did not affect these basal NE and Epi releases (Table 1). Dialysate NE and Epi concentrations increased by nerve stimulation and rapidly declined after the stimulation. Thus we subtracted the dialysate NE and Epi contents before stimulation from those during stimulation and expressed these values as indexes of NE and Epi releases induced by stimulation.

Effects of ω-conotoxin GVIA. ω-Conotoxin GVIA (10 μg/kg) significantly inhibited ACh release at 2 Hz from 6.2 ± 0.9 to 3.6 ± 0.5 nM, ACh release at 4 Hz from 12.2 ± 1.7 to 7.9 ± 1.2 nM, NE release at 4 Hz from 34 ± 6 to 17 ± 3 nM, Epi release at 2 Hz from 81 ± 13 to 42 ± 3 nM, and Epi release at 4 Hz from 180 ± 21 to 94 ± 7 nM. However, inhibition of NE release at 2 Hz was not statistically significant (Fig. 1*A*). A fivefold higher dose of ω-conotoxin GVIA (50 μg/kg) did not

Table 1. *Basal dialysate NE and Epi concentrations before and after administration of Ca^{2+} channel antagonists*

	NE, nM	Epi, nM
ω-Conotoxin GVIA (10 and 50 μg/kg) (n = 12)		
Before administration	4.9±0.9	20.6±2.9
After administration	3.8±0.6	21.0±2.6
ω-Conotoxin MVIIC (50 μg/kg) (n = 6)		
Before administration	4.1±1.0	20.2±2.6
After administration	4.6±0.9	24.0±3.5
ω-Conotoxin GVIA (50 μg/kg) + MVIIC (250 μg/kg) (n = 6)		
Before administration	4.4±1.3	17.5±3.8
After administration	3.1±0.7	20.8±4.4
Nifedipine (100 and 300 μg/kg) (n = 12)		
Before administration	4.0±0.6	17.4±2.2
After administration	3.3±0.9	17.7±2.9

Values are means ± SE; *n*, no. of rats. NE, norepinephrine; Epi, epinephrine.

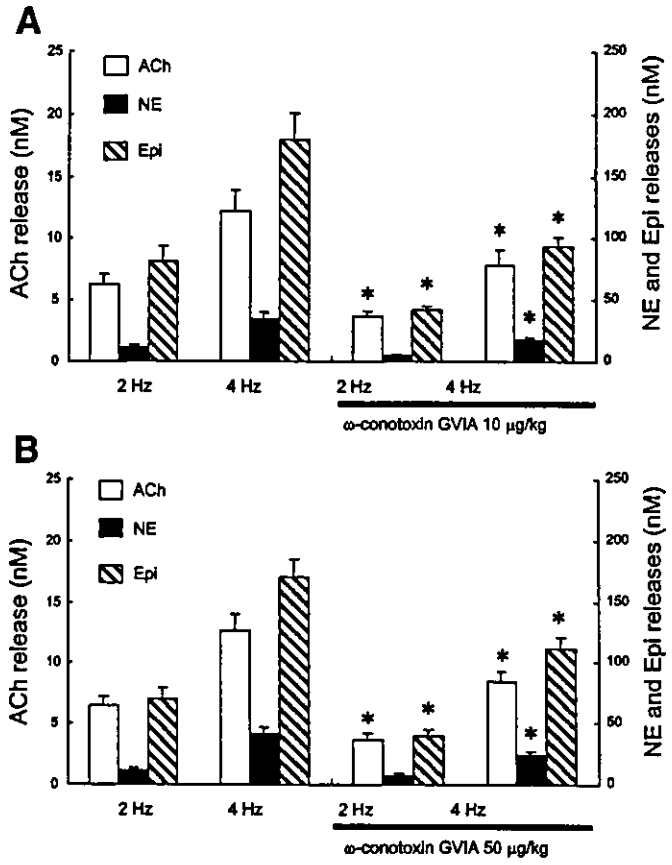

Fig. 1. Effects of ω-conotoxin GVIA on ACh, norepinephrine (NE), and epinephrine (Epi) releases. ω-Conotoxin GVIA (10 μg/kg) inhibited ACh release at 2 and 4 Hz, NE release at 4 Hz, and Epi release at 2 and 4 Hz (*A*). A 5-fold higher dose of ω-conotoxin GVIA (50 μg/kg) did not further inhibit these releases (*B*). Values are means ± SE from 6 rats. $*P < 0.05$ vs. ACh, NE, or Epi release at same frequency before administration.

further inhibit release. ω-Conotoxin GVIA (50 μg/kg) significantly inhibited ACh release at 2 Hz from 6.5 ± 0.7 to 3.7 ± 0.5 nM, ACh release at 4 Hz from 12.6 ± 1.4 to 8.5 ± 0.8 nM, NE release at 4 Hz from 41 ± 6 to 24 ± 4 nM, Epi release at 2 Hz from 70 ± 10 to 40 ± 6 nM, and Epi release at 4 Hz from 170 ± 15 to 112 ± 10 nM (Fig. 1*B*).

Effects of ω-conotoxin MVIIC. ω-Conotoxin MVIIC (50 μg/kg) significantly inhibited ACh release at 4 Hz from 11.7 ± 2.5 to 8.5 ± 2.1 nM and Epi release at 4 Hz from 170 ± 38 to 129 ± 35 nM. Inhibitions of ACh and Epi releases at 2 Hz and NE release at either frequency were not statistically significant (Fig. 2).

Effects of combined ω-conotoxin GVIA and MVIIC. Combined ω-conotoxin GVIA (50 μg/kg) and MVIIC (250 μg/kg) significantly inhibited ACh release at 2 Hz from 6.7 ± 0.6 to 1.9 ± 0.3 nM, ACh release at 4 Hz from 12.1 ± 1.3 to 3.8 ± 0.6 nM, NE release at 2 Hz from 11.1 ± 1.1 to 1.2 ± 0.3 nM, NE release at 4 Hz from 36 ± 5 to 8 ± 2 nM, Epi release at 2 Hz from 88 ± 9 to 13 ± 3 nM, and Epi release at 4 Hz from 187 ± 20 to 49 ± 9 nM (Fig. 3).

Effects of nifedipine. Nifedipine (300 μg/kg) did not change ACh release at either frequency but significantly inhibited Epi release at 4 Hz from 172 ± 31 to 135 ± 23 nM. Inhibitions of Epi release at 2 Hz and NE release at either frequency were not statistically significant (Fig. 4*A*). A threefold higher dose of

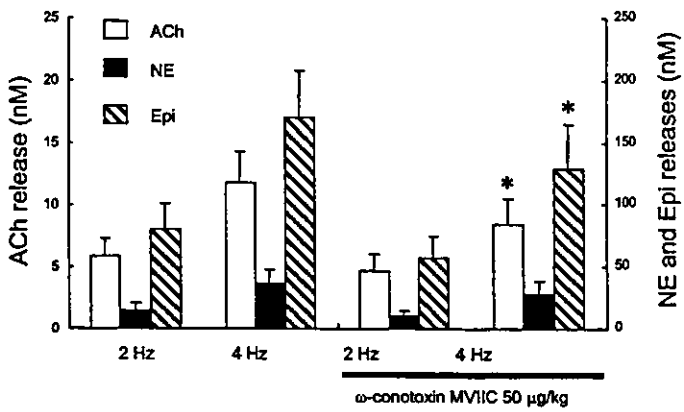

Fig. 2. Effects of ω-conotoxin MVIIC on ACh, NE, and Epi releases. ω-Conotoxin MVIIC (50 μg/kg) inhibited ACh and Epi releases at 4 Hz. Values are means ± SE from 6 rats. $*P < 0.05$ vs. ACh, NE, or Epi release at same frequency before administration.

nifedipine (900 μg/kg) did not change ACh release but significantly inhibited Epi release at 4 Hz from 188 ± 24 to 128 ± 15 nM and NE release at 4 Hz from 33 ± 5 to 24 ± 4 nM. Inhibitions of NE and Epi releases at 2 Hz were not statistically significant (Fig. 4*B*).

DISCUSSION

Effects of Ca^{2+} channel antagonists on ACh release from splanchnic nerve endings. In the present study, ω-conotoxin GVIA (10 μg/kg) inhibited ACh release at both 2 and 4 Hz by approximately 35–40%. A fivefold higher dose of ω-conotoxin GVIA (50 μg/kg) did not further inhibit ACh release. ω-Conotoxin MVIIC (50 μg/kg) inhibited ACh release at 4 Hz by ~30%. Combined ω-conotoxin GVIA (50 μg/kg) and MVIIC (250 μg/kg) inhibited ACh release at both 2 and 4 Hz by ~70%. N- and P/Q-type Ca^{2+} channels could be present on the splanchnic nerve endings and be involved in ACh release. P/Q-type Ca^{2+} channels may play a role in ACh release at a high frequency of stimulation. ACh release response was resistant to nifedipine (300 and 900 μg/kg) at both 2 and 4 Hz. L-type Ca^{2+} channels could not be present on splanchnic nerve

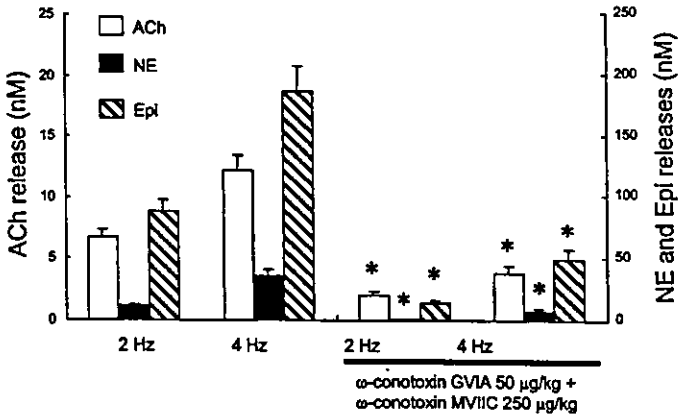

Fig. 3. Effects of combined ω-conotoxin GVIA and MVIIC on ACh, NE, and Epi releases. Combined ω-conotoxin GVIA (50 μg/kg) and MVIIC (250 μg/kg) inhibited ACh, NE, and Epi releases at 2 and 4 Hz. Values are means ± SE from 6 rats. $*P < 0.05$ vs. ACh, NE, or Epi release at same frequency before administration.

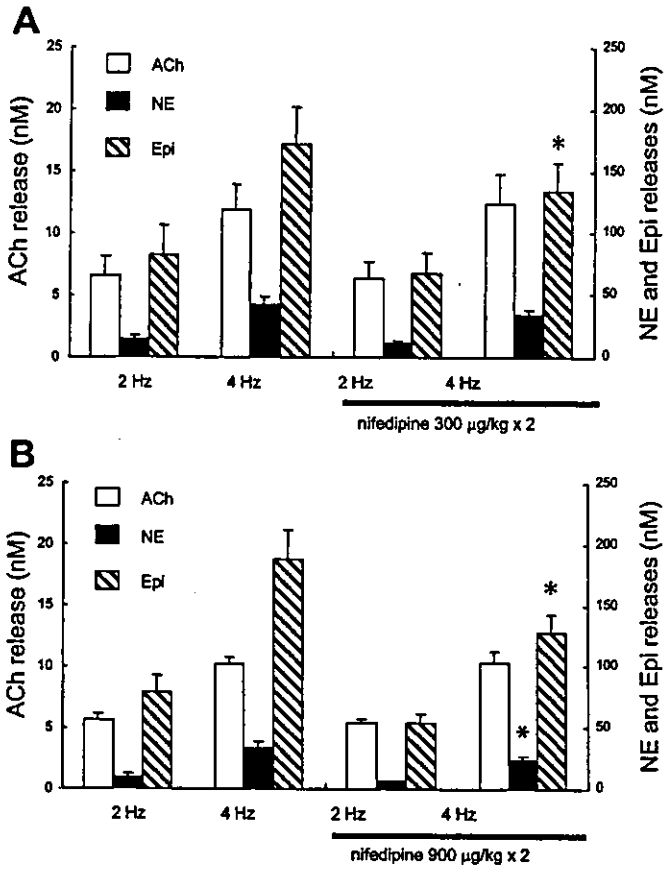

Fig. 4. Effects of nifedipine on ACh, NE, and Epi releases. Nifedipine (300 μg/kg) did not change ACh release at either frequency but inhibited Epi release at 4 Hz (*A*). Nifedipine (900 μg/kg) did not change ACh release at either frequency but inhibited NE and Epi releases at 4 Hz (*B*). Values are means ± SE from 6 rats. $*P < 0.05$ vs. ACh, NE, or Epi release at same frequency before administration.

endings or not play a major role in ACh release. This is the first direct study to demonstrate the type of Ca^{2+} channels controlling ACh release from splanchnic nerve endings.

In isolated rat adrenal glands, catecholamine release induced by field stimulation is sensitive to P/Q-type Ca^{2+} channel antagonist, whereas that induced by exogenous ACh is insensitive (27). This indirect study suggested the involvement of P/Q-type Ca^{2+} channels in ACh release but failed to show the involvement of N-type Ca^{2+} channels. In isolated bovine adrenal glands, a direct measurement study showed that a reduction of the extracellular Ca^{2+} concentration inhibits ^{3}H-labeled ACh release induced by field stimulation, but N- and L-type Ca^{2+} channel antagonists do not (28). Thus our findings are in part consistent with these direct and indirect studies but inconsistent as to the involvement of N-type Ca^{2+} channels.

This discrepancy might be ascribed to the experimental method. The contribution of Ca^{2+} channels may vary with the type of method used to evoke ACh release. In these studies, ACh release was evoked by electrical field stimulation of isolated adrenal glands, which is known to induce ACh release but not direct depolarization of chromaffin cells (34). In the present study, ACh release was evoked in the in vivo state by electrical stimulation of splanchnic nerves. The type of Ca^{2+} channels involved in ACh release may vary with the frequency, amplitude, or time period of stimulation. Actually, in the present study, we observed the involvement of P/Q-type Ca^{2+} channels at only high-frequency stimulation, while it has been reported in perfused rat adrenal glands that N-type Ca^{2+} channels are involved in the maintenance of catecholamine release in response to long splanchnic nerve stimulation (31). The time period of 2 min in the present study seems to be longer than those in earlier studies but could be within the physiological range. Moreover, the blocking action of ω-conotoxin GVIA is time dependent as well as dose dependent and irreversible (8, 11, 32, 36). The maximum functional effect of ω-conotoxin GVIA has been observed to be at least 15 min after administration. We evaluated the effect of ω-conotoxin GVIA 30 min after intravenous administration, when heart rate and mean arterial pressure had already been stabilized. The evaluation early after administration might lead to underestimation of the inhibitory effects of ω-conotoxin GVIA.

There are many similarities between synaptic transmission from splanchnic nerves to chromaffin cells and sympathetic ganglionic transmission (17). In isolated guinea pig paravertebral ganglia, an electrophysiological study has shown that both N- and P-type Ca^{2+} channel antagonists reduce cholinergic synaptic conductance, whereas L-type Ca^{2+} channel antagonist does not (19). In isolated rat superior cervical ganglia, both N- and P-type Ca^{2+} channel antagonists inhibit the rise in Ca^{2+} concentration in the terminal boutons (22). Moreover, in isolated rat superior cervical ganglia, ^{3}H-labeled ACh release induced by high K^+ is inhibited by both N- and P-type Ca^{2+} channel antagonists but unaffected by L-type Ca^{2+} channel antagonist (15). Our findings are similar to these findings obtained from isolated sympathetic preganglionic nerves.

The inhibition by ω-conotoxin GVIA (50 μg/kg) was almost the same as that by ω-conotoxin GVIA (10 μg/kg). Moreover, the inhibition by combined ω-conotoxin GVIA (50 μg/kg) and MVIIC (250 μg/kg) was almost algebraically the sum of the individual inhibition by ω-conotoxin GVIA (10 μg/kg) and MVIIC (50 μg/kg). These results suggest that fivefold higher doses of ω-conotoxin GVIA and MVIIC are sufficient to cause inhibition of Ca^{2+} channels. However, ~30% of ACh release was resistant to combined ω-conotoxin GVIA (50 μg/kg) and MVIIC (250 μg/kg). Other types of Ca^{2+} channels except for N- and P/Q-types may be involved in ACh release from splanchnic nerve endings. Further examination could be needed.

Effects of Ca^{2+} channel antagonists on catecholamine release from chromaffin cells. In the present study, nifedipine (300 μg/kg) did not change ACh release at 2 and 4 Hz but inhibited Epi release at 4 Hz by ~20%. A threefold higher dose of nifedipine (900 μg/kg) did not change ACh release at 2 and 4 Hz but inhibited NE and Epi releases at 4 Hz by ~30%. Adrenal chromaffin cells are divided into two populations: NE- and Epi-storing cells (10). L-type Ca^{2+} channels could be present on the surface of both NE- and Epi-storing cells and play a role in NE and Epi releases.

Approximately 70% of catecholamine release was resistant to nifedipine (900 μg/kg). This result suggests that other types of Ca^{2+} channels except for L-type are present on chromaffin cells and involved in NE and Epi releases, although we cannot exclude the possibility of incomplete inhibition of L-type Ca^{2+} channels. Species differences in the types of Ca^{2+} channels controlling Ca^{2+} influx and catecholamine release have been

shown with rat, cat, and bovine chromaffin cells (5, 6, 13, 24). In patch-clamp studies of isolated rat chromaffin cells, Ca^{2+} inward current elicited by depolarization is sensitive to both L- and N-type Ca^{2+} channel antagonists (16, 21). The study measuring Ba^{2+} current by patch-clamp technique has shown the existence of L-, N-, and P/Q-type Ca^{2+} channels on rat chromaffin cells and the following distribution of Ca^{2+} channels in decreasing order: L-type > N-type > P/Q-type (13). In the present study, ω-conotoxin GVIA (10 and 50 μg/kg) inhibited NE release at 4 Hz and Epi release at 2 and 4 Hz by approximately 45–50%. ω-Conotoxin MVIIC (50 μg/kg) inhibited Epi release at 4 Hz by ~30%. Combined ω-conotoxin GVIA (50 μg/kg) and MVIIC (250 μg/kg) inhibited NE and Epi releases at 2 and 4 Hz by approximately 75–85%. However, these Ca^{2+} channel antagonists simultaneously inhibited ACh release to almost the same extent. It is difficult to determine how much Ca^{2+} antagonists are acting on chromaffin cells when Ca^{2+} channel antagonists inhibit ACh release. Thus, although much of these inhibitions of catecholamine release may be considered to be consequences of the inhibition of ACh release, we cannot exclude the possibility that N- or P/Q-type Ca^{2+} channels may be involved in the in vivo catecholamine release on chromaffin cells.

The inhibition of NE release at 2 Hz by ω-conotoxin GVIA (10 and 50 μg/kg) and the inhibition of NE release at 4 Hz by ω-conotoxin MVIIC (50 μg/kg) were not statistically significant despite significant inhibitions of ACh and Epi releases. In the same preparation, we have shown that cholinergic antagonists almost inhibited NE and Epi releases induced by nerve stimulation (1, 2). However, the correlation between ACh and NE releases was poorer than that between ACh and Epi releases when stimulation frequency was raised stepwise (2). Insignificant inhibitions of NE release may be ascribed to this poor correlation.

In the present study, Ca^{2+} channel antagonists did not affect basal dialysate NE and Epi levels. In our previous study of the same preparation, these basal levels were not affected by neostigmine, hexamethonium, or atropine (1). We then concluded that these basal dialysate NE and Epi levels reflect noncholinergic catecholamine release. N-, P/Q-, and L-type Ca^{2+} channels may not play a major role in basal noncholinergic catecholamine release from adrenal medulla.

Methodological considerations. We administered neostigmine locally to adrenal medulla through a dialysis probe. Cholinesterase inhibitor was necessary to monitor endogenous ACh even during splanchnic nerve stimulation because released ACh is rapidly degraded by acetylcholinesterase before reaching the dialysis fiber. In the same preparation, local administration of neostigmine enhanced the dialysate catecholamine response to nerve stimulation by approximately threefold, but dialysate ACh and catecholamine responses are correlated with the stimulation frequency of splanchnic nerves in the presence of neostigmine (2). Thus dialysate ACh and catecholamine responses are likely to be correlated with the amount of Ca^{2+} influx from voltage-dependent Ca^{2+} channels even in the presence of neostigmine.

Intravenous administration of Ca^{2+} channel antagonists induced changes in heart rate or mean arterial pressure. These changes might affect ACh and catecholamine releases through a baroreflex mechanism. Moreover, these hemodynamic changes might decrease the spillover of ACh or catecholamine from adrenal medulla and affect the dialysate ACh or catecholamine concentrations (20). In our preparation, however, splanchnic nerves had been transected before control sampling, and basal dialysate catecholamine concentrations did not change before or after administration. Thus effects of these hemodynamic changes could be negligible when we considered the effects of Ca^{2+} channel antagonists on nerve stimulation-induced dialysate responses.

In conclusion, we applied dialysis technique to the adrenal medulla of anesthetized rats and investigated the effects of Ca^{2+} channel antagonists on ACh and catecholamine releases induced by electrical stimulation of splanchnic nerves. Both N- and P/Q-type Ca^{2+} channels control ACh release on preganglionic splanchnic nerve endings while L-type Ca^{2+} channels do not. L-type Ca^{2+} channels are involved in norepinephrine and epinephrine releases on chromaffin cells.

GRANTS

This study was supported by the Program for Promotion of Fundamental Studies in Health Science of the Organization for Pharmaceutical Safety and Research (of Japan); by a Health Sciences Research Grant for Advanced Medical Technology from the Ministry of Health and Welfare of Japan; by a Ground-Based Research Grant for the Space Utilization promoted by the National Space Development Agency of Japan and Japan Space Forum; and by grants-in-aid for scientific research from the Ministry of Education, Science.

REFERENCES

1. **Akiyama T, Yamazaki T, Mori H, and Sunagawa K.** Inhibition of cholinesterase elicits muscarinic receptor-mediated synaptic transmission in the rat adrenal medulla. *Auton Neurosci* 107: 65–73, 2003.
2. **Akiyama T, Yamazaki T, Mori H, and Sunagawa K.** Simultaneous monitoring of acetylcholine and catecholamine release in the in vivo rat adrenal medulla. *Neurochem Int* 44: 497–503, 2004.
3. **Akiyama T, Yamazaki T, and Ninomiya I.** In vivo detection of endogenous acetylcholine release in cat ventricles. *Am J Physiol Heart Circ Physiol* 266: H854–H860, 1994.
4. **Akiyama T, Yamazaki T, and Ninomiya I.** In vivo monitoring of myocardial interstitial norepinephrine by dialysis technique. *Am J Physiol Heart Circ Physiol* 261: H1643–H1647, 1991.
5. **Albillos A, Artalejo AR, López MG, Gandía L, García AG, and Carbone E.** Calcium channel subtypes in cat chromaffin cells. *J Physiol* 477: 197–213, 1994.
6. **Artalejo CR, Perlman RL, and Fox AP.** ω-Conotoxin GVIA blocks a Ca^{2+} current in bovine chromaffin cells that is not of the "classic" N type. *Neuron* 8: 85–95, 1992.
7. **Buckingham RE.** Studies on the anti-vasoconstrictor activity of BRL 34915 in spontaneously hypertensive rats; a comparison with nifedipine. *Br J Pharmacol* 93: 541–552, 1988.
8. **Clasbrummel B, Osswald H, and Illes P.** Inhibition of noradrenaline release by ω-conotoxin GVIA in the rat tail artery. *Br J Pharmacol* 96: 101–110, 1989.
9. **Coupland RE.** *The Natural History of the Chromaffin Cell.* London: Longmans, 1965.
10. **Coupland RE.** Ultrastructural features of the mammalian adrenal medulla. In: *Ultrastructure of Endocrine Cells and Tissues,* edited by Motta PM. Boston, MA: Nijhoff, 1984, p. 168–179.
11. **De Luca A, Li CG, Rand MJ, Reid JJ, Thaina P, and Wong-Dusting HK.** Effects of ω-conotoxin GVIA on autonomic neuroeffector transmission in various tissues. *Br J Pharmacol* 101: 437–447, 1990.
12. **Dunlap K, Luebke JI, and Turner TJ.** Exocytotic Ca^{2+} channels in mammalian central neurons. *Trends Neurosci* 18: 89–98, 1995.
13. **Gandía L, Borges R, Albillos A, and García AG.** Multiple calcium channel subtypes in isolated rat chromaffin cells. *Pflügers Arch* 430: 55–63, 1995.
14. **Gaspo R, Yamaguchi N, and de Champlain J.** Nifedipine inhibits adrenal but not circulating catecholamine response to nicotinic stimulation in dogs. *Am J Physiol Regul Integr Comp Physiol* 267: R1545–R1551, 1994.
15. **Gonzalez Burgos GR, Biali FI, Cherksey BD, Sugimori M, Llinas RR, and Uchitel OD.** Different calcium channels mediate transmitter release

evoked by transient or sustained depolarization at mammalian sympathetic ganglia. *Neuroscience* 64: 117–123, 1995.

16. **Hollins B and Ikeda SR.** Inward currents underlying action potentials in rat adrenal chromaffin cells. *J Neurophysiol* 76: 1195–1211, 1996.
17. **Holman ME, Coleman HA, Tonta MA, and Parkington HC.** Synaptic transmission from splanchnic nerves to the adrenal medulla of guinea-pigs. *J Physiol* 478: 115–124, 1994.
18. **Hillyard DR, Monje VD, Mintz IM, Bean BP, Nadasdi L, Ramachandran J, Miljanich G, Azimi-Zoonooz A, McIntosh JM, Cruz LJ, Imperial JS, and Olivera BM.** A new Conus peptide ligand for mammalian presynaptic Ca^{2+} channels. *Neuron* 9: 69–77, 1992.
19. **Ireland DR, Davies PJ, and McLachlan EM.** Calcium channel subtypes differ at two types of cholinergic synapse in lumbar sympathetic neurones of guinea-pigs. *J Physiol* 514: 59–69, 1999.
20. **Kawada T, Yamazaki T, Akiyama T, Shishido T, Inagaki M, Uemura K, Miyamoto T, Sugimachi M, Takaki H, and Sunagawa K.** In vivo assessment of acetylcholine-releasing function at cardiac vagal nerve terminals. *Am J Physiol Heart Circ Physiol* 281: H139–H145, 2001.
21. **Kim SJ, Lim W, and Kim J.** Contribution of L- and N-type calcium currents to exocytosis in rat adrenal medullary chromaffin cells. *Brain Res* 675: 289–296, 1995.
22. **Lin YQ, Brain KL, and Bennett MR.** Calcium in sympathetic boutons of rat superior cervical ganglion during facilitation, augmentation and potentiation. *J Auton Nerv Syst* 73: 26–37, 1998.
23. **Lomax RB, Michelrna P, Núñez L, García-Sancho J, García AG, and Montiel C.** Different contributions of L- and Q-type Ca^{2+} channels to Ca^{2+} signals and secretion in chromaffin cell subtypes. *Am J Physiol Cell Physiol* 272: C476–C484, 1997.
24. **López MG, Albillos A, de la Fuente MT, Borges R, Gandía L, Carbone E, García AG, and Artalejo AR.** Localized L-type calcium channels control exocytosis in cat chromaffin cells. *Pflügers Arch* 427: 348–354, 1994.
25. **Meir A, Ginsburg S, Butkevich A, Kachalsky SG, Kaiserman I, Ahdut R, Demirgoren S, and Rahamimoff R.** Ion channels in presynaptic nerve terminals and control of transmitter release. *Physiol Rev* 79: 1019–1088, 1999.
26. **Morimoto H, Matsuda A, Ohori M, and Fujii T.** Effects of ω-conotoxin GVIA on the activation of capsaicin-sensitive afferent sensory nerves in guinea pig airway tissues. *Jpn J Pharmacol* 71: 161–166, 1996.
27. **Nagayama T, Matsumoto T, Kuwakubo F, Fukushima Y, Yoshida M, Suzuki-Kusaba M, Hisa H, Kimura T, and Satoh S.** Role of calcium channels in catecholamine secretion in the rat adrenal gland. *J Physiol* 520: 503–512, 1999.
28. **O'Farrell M, Ziogas J, and Marley PD.** Effects of N- and L-type calcium channel antagonists and (±)-Bay K8644 on nerve-induced catecholamine secretion from bovine perfused adrenal glands. *Br J Pharmacol* 121: 381–388, 1997.
29. **Pruneau D and Belichard P.** Haemodynamic and humoral effects of ω-conotoxin GVIA in normotensive and spontaneously hypertensive rats. *Eur J Pharmacol* 211: 329–335, 1992.
30. **Randall A and Tsien RW.** Pharmacological dissection of multiple types of Ca^{2+} channel currents in rat cerebellar granule neurons. *J Neurosci* 15: 2995–3012, 1995.
31. **Santana F, Michelena P, Jaén R, García AG, and Borges R.** Calcium channel subtypes and exocytosis in chromaffin cells: a different view from the intact rat adrenal. *Naunyn Schmiedebergs Arch Pharmacol* 360: 33–37, 1999.
32. **Serone AP and Angus JA.** Role of N-type calcium channels in autonomic neurotransmission in guinea-pig isolated left atria. *Br J Pharmacol* 127: 927–934, 1999.
33. **Smith AB and Cunnane TC.** Multiple calcium channels control neurotransmitter release from rat postganglionic sympathetic nerve terminals. *J Physiol* 499: 341–349, 1997.
34. **Wakade AR.** Studies on secretion of catecholamines evoked by acetylcholine or transmural electrical stimulation of the rat adrenal gland. *J Physiol* 313: 463–480, 1981.
35. **Winer BJ.** *Statistical Principles in Experimental Design* (2nd ed.). New York: McGraw-Hill, 1971.
36. **Wright CE and Angus JA.** Prolonged cardiovascular effects of the N-type Ca^{2+} channel antagonist omega-conotoxin GVIA in conscious rabbits. *J Cardiovasc Pharmacol* 30: 392–399, 1997.
37. **Yahagi N, Akiyama T, and Yamazaki T.** Effects of ω-conotoxin GVIA on cardiac sympathetic nerve function. *J Auton Nerv Syst* 68: 43–48, 1998.

Available online at www.sciencedirect.com
SCIENCE DIRECT®
ELSEVIER
Journal of Electron Spectroscopy and Related Phenomena 137–140 (2004) 699–704
JOURNAL OF ELECTRON SPECTROSCOPY and Related Phenomena
www.elsevier.com/locate/elspec

Portable X-ray generator utilizing a cerium-target radiation tube for angiography

E. Sato[a,*], Y. Hayasi[a], R. Germer[b], E. Tanaka[c], H. Mori[d], T. Kawai[e], T. Ichimaru[f], S. Sato[g], K. Takayama[h], H. Ido[i]

[a] *Department of Physics, Iwate Medical University, Morioka 020-0015, Japan*
[b] *ITP, FHTW FB1 and TU-Berlin, D 12249 Berlin, Germany*
[c] *Department of Nutritional Science, Faculty of Applied Bio-science, Tokyo University of Agriculture, Setagayaku 156-8502, Japan*
[d] *Department of Cardiac Physiology, National Cardiovascular Center Research Institute, Osaka 565-8565, Japan*
[e] *Electron Tube Division #2, Hamamatsu Photonics Inc., Iwata-gun 438-0193, Japan*
[f] *Department of Radiological Technology, School of Health Sciences, Hirosaki University, Hirosaki 036-8564, Japan*
[g] *Department of Microbiology, School of Medicine, Iwate Medical University, Morioka 020-8505, Japan*
[h] *Shock Wave Research Center, Institute of Fluid Science, Tohoku University, Sendai 980-8577, Japan*
[i] *Department of Applied Physics and Informatics, Faculty of Engineering, Tohoku Gakuin University, Tagajo 985-8537, Japan*

Available online 15 April 2004

Abstract

The development of a portable X-ray generator with a cerium-target tube and its application to angiography are described. The portable X-ray generator consists of a main controller, a unit with a Cock–Croft circuit and an X-ray tube, and a personal computer. Negative high voltages are applied to the cathode electrode in the X-ray tube, and the tube voltage and current are regulated by the controller or the computer. The X-ray tube is a glass-enclosed double-focus diode with a cerium target and a 0.5 mm-thick beryllium window. The maximum tube voltage and current were 60 kV and 0.8 mA, respectively. The focal-spot sizes were 4 mm × 4 mm (large) and 1 mm × 1 mm (small), respectively. Angiography was performed with a computed radiography system using iodine-based microspheres. The tube voltage, the current, the distance between the imaging plate and the X-ray source, and the spot size were 60 kV, 0.4 mA, 1.5 m, and small, respectively. In this angiography, we observed coronary arteries and fine blood vessels of about 50 μm or less with high contrasts.

Keywords: Cerium-target X-ray tube; Cerium characteristic X-rays; K-absorption edge; High contrast angiography; Microangiogrphy

1. Introduction

In conjunction with single crystals, synchrotrons generate monochromatic X-rays. These rays play an important role in parallel radiography and have been employed to perform high-contrast micro-angiography [1] and phase imaging [2–4]. However, it is difficult to obtain sufficient machine times for various research projects including medical applications.

So far, several different flash X-ray generators have been developed [5,6], and soft generators [7–12] with photon energies of lower than 150 keV can be employed to perform biomedical radiography. In order to produce monochromatic X-rays, plasma flash X-ray generators [13–16] are useful, since quite intense and sharp characteristic X-rays such as lasers have been produced from weakly ionized linear plasmas of nickel, copper and molybdenum, while bremsstrahlung rays are hardly detected at all. Using these generators, the characteristic X-ray intensity substantially increased with corresponding increases in the charging voltage.

Since K-series characteristic X-rays from cerium target are absorbed effectively by iodine-based contrast mediums, a cerium-target X-ray tube is very useful in order to perform high-contrast angiography. On the other hand, cerium is a rare earth element and has a high reactivity, and it is difficult to design the target. However, the development of a cerium-target tube for high-contrast angiography has long been wished for.

* Corresponding author.
E-mail address: dresato@iwate-med.ac.jp (E. Sato).

0368-2048/$ – see front matter © 2004 Elsevier B.V. All rights reserved.
doi:10.1016/j.elspec.2004.02.011

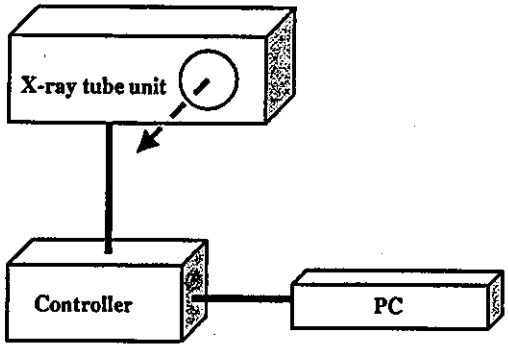

Fig. 1. Block diagram of the portable X-ray generator with a cerium-target radiation tube, which is specially used for angiography using iodine-based contrast mediums. The negative high voltage is applied to the cathode electrode, and the tube current is regulated by the filament temperature. Although the X-ray tube is a double-focus type, we usually employ a small focus in order to measure the radiographic characteristics and to perform angiography.

In the present research, we developed a portable X-ray generator with a cerium-target tube, used to perform preliminary study on angiography achieved with cerium K-series characteristic X-rays.

2. Generator

Fig. 1 shows the block diagram of the X-ray generator, which consists of a main controller, an X-ray tube unit with a Cockcroft circuit and a cerium-target tube, and a personal computer. The negative high-voltage is applied to the cathode electrode, and the anode (target) is connected to the ground potential. In this experiment, the tube voltage was regulated from 40 to 65 kV, and the tube current was regulated within 0.8 mA by the filament temperature. The exposure time is controlled in order to obtain optimum X-ray intensity, and the X-ray tube is a double-focus type with focal-spot dimensions of approximately 4 mm × 4 mm (large spot) and 1 mm × 1 mm (small spot), respectively. The maximum tube current is determined by the spot dimensions, and the currents of small and large spots are 0.4 and 0.8 mA, respectively.

3. Characteristics

3.1. X-ray intensity

X-ray intensity was measured by a Victoreen 660 ionization chamber at 1.0 m from the X-ray source using a small spot with an exposure time of 1.0 s (Fig. 2). At a constant tube current of 40 μA, the X-ray intensity increased when the tube voltage was increased. The intensity was roughly in proportion to the tube current at a constant tube voltage of 60 kV. In this measurement, the intensity with a tube voltage of 60 kV and a current of 90 μA was 2.14 μC/kg at 1.0 m from the source with errors of less than 0.2%.

3.2. X-ray source

In order to measure images of the X-ray source, we employed a pinhole camera with a hole diameter of 50 μm in conjunction with a computed radiography (CR) system (Fig. 3) [17]. When the tube voltage was increased, the spot intensity increased slightly, and spot dimensions seldom varied and had values of approximately 1 mm × 1 mm.

3.3. X-ray spectra

In order to measure X-ray spectra, we employed a cadmium tellurium detector (CDTE2020X, Hamamatsu Photonics Inc.) (Fig. 4). Compared with a germanium detector, this detector has lower energy resolutions. When the tube voltage was increased, both the characteristic X-ray intensity and the maximum photon energy of bremsstrahlung X-rays increased. According to insertion of a monochromatic cerium oxide filter, quasi-monochromatic X-rays were obtained.

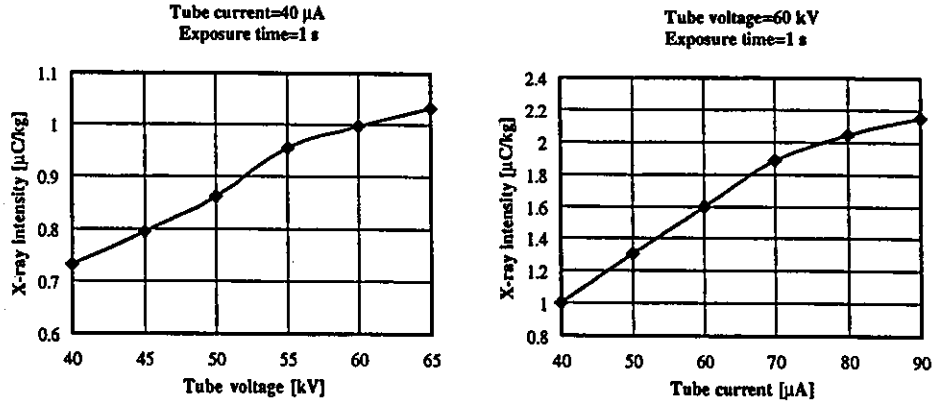

Fig. 2. X-ray intensity measured at 1.0 m from the X-ray source according to changes in the tube voltage and current. In the measurement, we employed an ionization chamber without using a monochromatic filter.

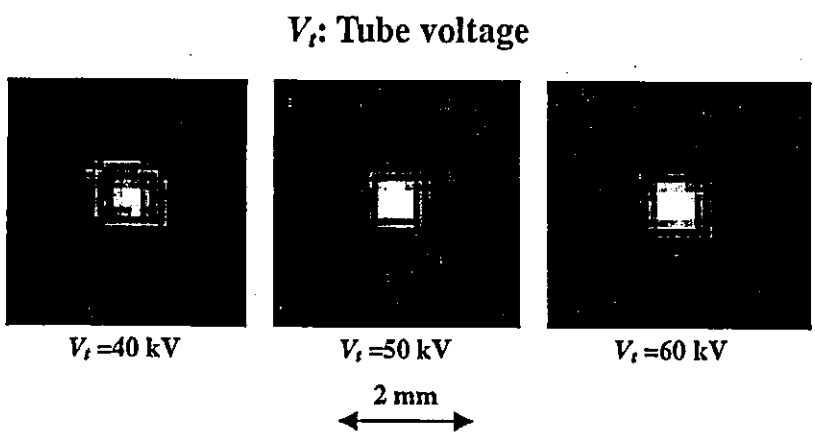

Fig. 3. Images of the X-ray source measured by a 100 mm diameter pinhole with changes in the tube voltage.

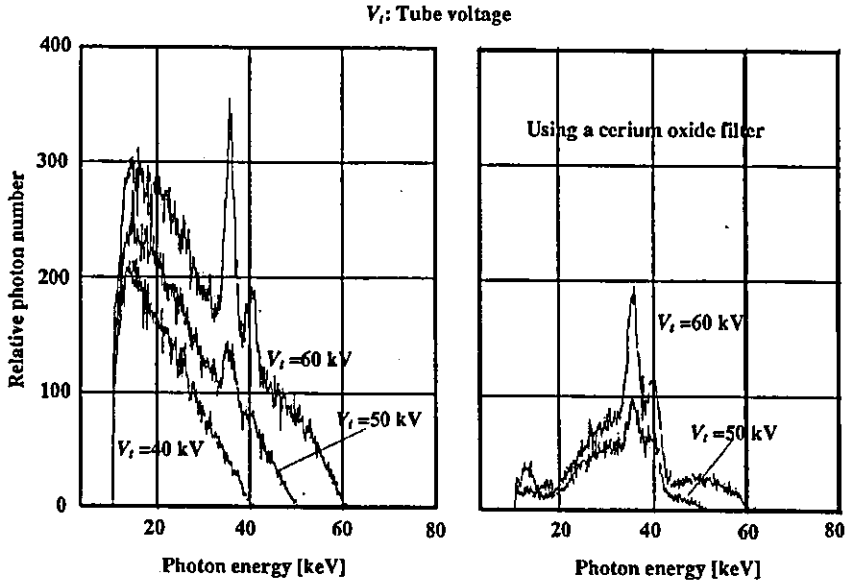

Fig. 4. X-ray spectra measured by a cadmium tellurium detector with changes in the tube voltage.

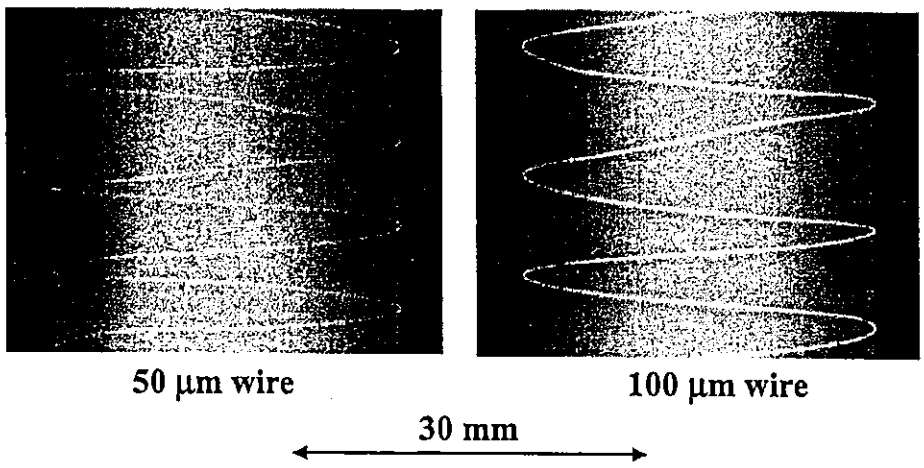

Fig. 5. Radiograms of tungsten wires around a rod made of PMMA used for estimating the image resolution.

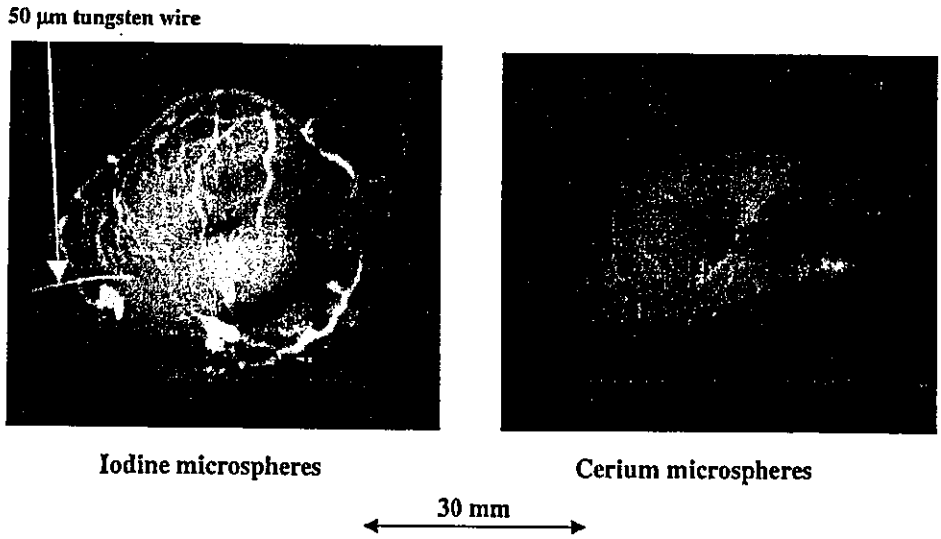

Fig. 6. Angiograms of rabbit hearts using (a) iodine and (b) cerium microspheres.

4. Angiography

The angiography was performed by a CR system (Konica Regius 150) using the monochromatic filter, and the distance (between the X-ray source and the imaging plate) and the tube voltage were 1.5 m and 60 kV, respectively.

Firstly, rough measurements of image resolution were made using wires. Fig. 5 shows radiograms of tungsten wires coiled around rods made of polymethyl methacrylate (PMMA). Although the image contrast increased with increases in the wire diameter, a 50 μm diameter wire could be observed.

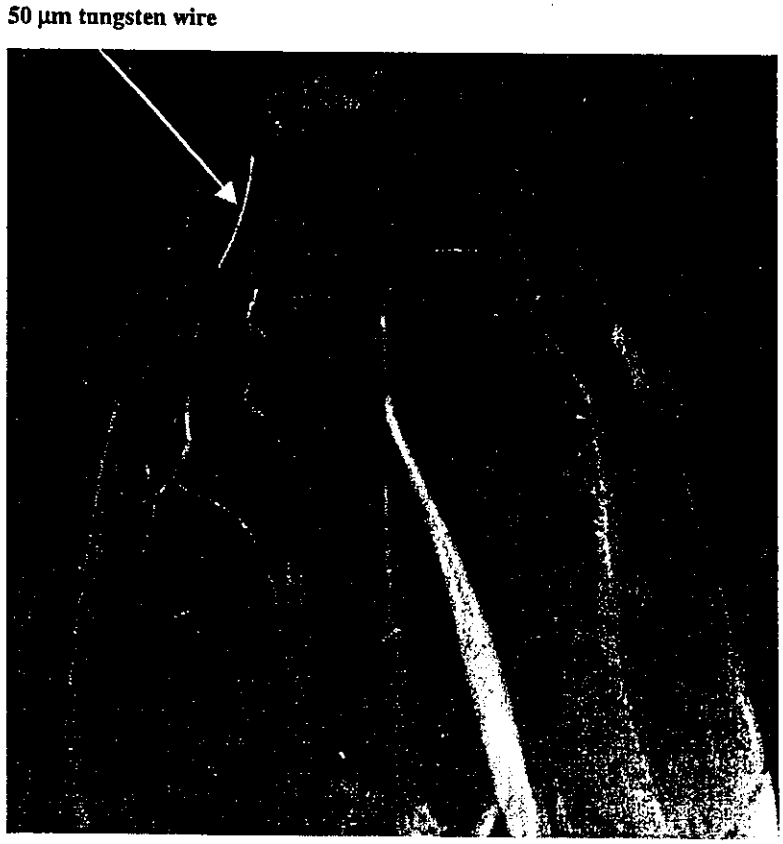

Fig. 7. Angiograms of the external ear of a rabbit using iodine-based microspheres. In this angiography, we employed a 50 μm tungsten wire to roughly determine the diameters of blood vessels.

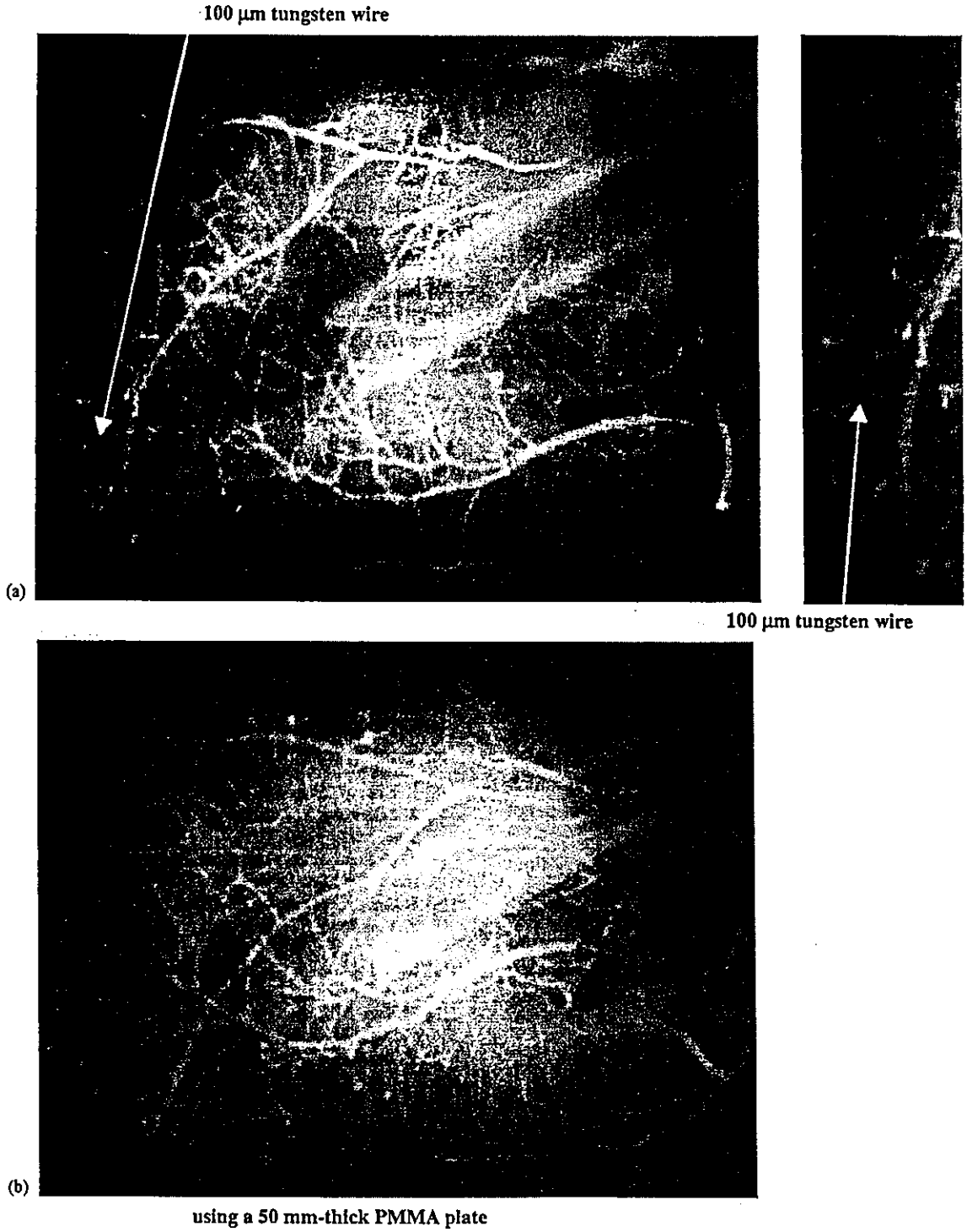

Fig. 8. Angiograms of an extracted heart of a dog. (a) Normal image and (b) image using a 50 mm PMMA plate set in front of the heart, facing the X-ray source.

Angiograms of rabbit hearts are shown in Fig. 6. These two images were obtained using iodine and cerium microspheres of 15 μm in diameter. In case where the cerium spheres were employed, the coronary arteries were barely visible. Fig. 7 shows an angiogram of the external ear of a rabbit using iodine spheres, and fine blood vessels of about 50 μm are clearly visible. In angiography of a larger heart extracted from a dog, using iodine spheres, a 50 mm thick PMMA plate was set in front of the heart facing X-ray source, and image contrast of coronary arteries decreased slightly with increases in the plate thickness (Fig. 8).